The FEBS Journal

FEBS PRESS science publishing by scientists

Sphingosine 1-phosphate attenuates neuronal dysfunction induced by amyloid-β oligomers through endocytic internalization of NMDA receptors

Alessandra Bigi, Roberta Cascella, Giulia Fani, Caterina Bernacchioni, Francesca Cencetti, Paola Bruni, Fabrizio Chiti, Chiara Donati and Cristina Cecchi

Department of Experimental and Clinical Biomedical Sciences, University of Florence, Italy

Keywords
Alzheimer's disease; calcium dyshomeostasis; misfolded protein oligomers; sphingolipid; sphingosine 1-phosphate receptors

Correspondence
C. Donati and C. Cecchi, Department of Experimental and Clinical Biomedical Sciences, University of Florence, Florence, Italy
Tel: +39 055 2751232 (CD); +39 055 2751222 (CC)
E-mails: chiara.donati@unifi.it (CD); cristina.cecchi@unifi.it (CC)

Alessandra Bigi and Roberta Cascella contributed equally to this article

(Received 12 January 2022, revised 24 May 2022, accepted 18 July 2022)

doi:10.1111/febs.16579

Soluble oligomers arising from the aggregation of the amyloid beta peptide (Aβ) have been identified as the main pathogenic agents in Alzheimer's disease (AD). Prefibrillar oligomers of the 42-residue form of Aβ ($A\beta_{42}O$) show membrane-binding capacity and trigger the disruption of Ca^{2+} homeostasis, a causative event in neuron degeneration. Since bioactive lipids have been recently proposed as potent protective agents against Aβ toxicity, we investigated the involvement of sphingosine 1-phosphate (S1P) signalling pathway in Ca^{2+} homeostasis in living neurons exposed to $A\beta_{42}O$. We show that both exogenous and endogenous S1P rescued neuronal Ca^{2+} dyshomeostasis induced by toxic $A\beta_{42}O$ in primary rat cortical neurons and human neuroblastoma SH-SY5Y cells. Further analysis revealed a strong neuroprotective effect of $S1P_1$ and $S1P_4$ receptors, and to a lower extent of $S1P_3$ and $S1P_5$ receptors, which activate the G_i-dependent signalling pathways, thus resulting in the endocytic internalization of the extrasynaptic GluN2B-containing *N*-methyl-*D*-aspartate receptors (NMDARs). Notably, the S1P beneficial effect can be sustained over time by sphingosine kinase-1 overexpression, thus counteracting the down-regulation of the S1P signalling induced by $A\beta_{42}O$. Our findings disclose underlying mechanisms of S1P neuronal protection against harmful $A\beta_{42}O$, suggesting that S1P and its signalling axis can be considered promising targets for therapeutic approaches for AD.

Introduction

Alzheimer's disease (AD) is a devastating and fatal neurodegenerative condition affecting ca. 35 million people worldwide. The amyloid hypothesis proposes that the cardinal pathological feature of AD is the presence of senile plaques in the brain of affected people, predominantly formed by the misfolded and self-assembled Aβ [1]. The aggregation process of Aβ is extremely complex and produces a large variety of oligomers, protofibrils and fibrils [2,3]. Soluble $A\beta_{42}O$ formed early during Aβ aggregation, through secondary nucleation or released from mature fibrils, are considered to be the most potent Aβ neurotoxins implicated in AD [3–5].

Increasing evidence suggests that the dysregulation of cytosolic Ca^{2+} homeostasis is an upstream event evoked by $A\beta_{42}O$ in cultured neuronal cells and in

Abbreviations
AD, Alzheimer's disease; Aβ, amyloid beta peptide; $A\beta_{42}M$, monomeric peptide; $A\beta_{42}O$, Aβ oligomers; BDNF, brain-derived neurotrophic factor; DMEM, Dulbecco's modified Eagle's medium; EMA, European Medicine Agency; FDA, American Food Drug Agency; HEPES, (2-hydroxyethyl) piperazine-1-ethanesulfonic acid; mem, memantine; MTT, 3-(4,5-dimethylthiazol-2-yl)-2,5 diphenyltetrazolium bromide; NMDARs, *N*-methyl-*D*-aspartate receptors; PTX, Pertussis toxin; S1P, sphingosine 1-phosphate; SK, sphingosine kinases; SPL, S1P lyase; Spns2, specific transporter spinster homologue 2; SPP1, S1P phosphatases 1.

relevant mouse AD models, where Ca^{2+} ions flow from the extracellular space to the cytosol [6–12]. In addition, the Ca^{2+} overload has been coupled to the deposition of senile plaques, as it appears to be most pronounced in the immediate vicinity of amyloid deposits in transgenic mouse models [13]. Furthermore, increased cytosolic Ca^{2+} levels can promote Aβ production and the microtubule-associated protein tau phosphorylation, implicating calcium dysfunction as a possible causative factor in AD [8,9].

The abnormal Ca^{2+} entry in cells arises from the $A\beta_{42}O$ ability to destabilize the cell membrane [8], as well as to activate a number of calcium channels, including the voltage-gated calcium channels [14,15] and receptor-operated channels such as glutamatergic *N*-methyl-*D*-aspartate receptors (NMDARs) [10,16–18]. In particular, the abnormal activation of extrasynaptic NMDARs, predominantly composed of the GluN2B subunit, is considered a crucial mechanism in the $A\beta_{42}O$-induced neurotoxicity, responsible for synaptic dysfunction [19]. Consistently, the blockade of GluN2B-containing NMDARs with specific antagonists, as well as the deletion of this subunit, were able to rescue Aβ-induced neurotoxicity [20,21]. In this regard, one of the drugs approved by the American Food Drug Agency (FDA), the European Medicine Agency (EMA), and other regulatory agencies is memantine (mem), which targets mainly extrasynaptic NMDARs as opposed to synaptic receptors [22].

Sphingosine 1-phosphate (S1P) is a potent bioactive sphingolipid involved in the regulation of cellular Ca^{2+} signals along with differentiation, stress resistance, survival and regulation of neurotransmitter release in the central nervous system [23,24]. S1P is synthetized by sphingosine phosphorylation, catalysed by sphingosine kinases (SK) 1 and 2 and is catabolized irreversibly by S1P lyase (SPL), or through the reversible dephosphorylation to sphingosine, catalysed by S1P phosphatases 1 (SPP1) and 2 (SPP2) [25,26]. Although SK1 and SK2 catalyse the same reaction, their different intracellular localization, kinetic properties and tissue distribution are responsible in some cases for different, even opposite, biological outcomes [25]. S1P can function as an intracellular messenger, or be released in the extracellular space via the specific transporter spinster homologue 2 (Spns2) [27]. Once outside the cells, S1P acts as a ligand of five distinct G protein-coupled receptors S1PR, referred to as $S1P_{1–5}$ [28].

A significant reduction in S1P levels was evident in the hippocampus of elderly people, suggesting that its loss can predispose them to neurodegeneration [29]. Notably, a decreased level of S1P has also been observed in the brain of AD patients with a negative correlation with the amount of aggregated Aβ [30,31]. Significant dysregulation of $S1P_1$ expression, the most represented S1P receptor in the brain, was also reported to be associated with the defective S1P signalling evoked by Aβ accumulation [32]. Recently, an S1P analogue named fingolimod (FTY720), currently used in the therapy of multiple sclerosis, was observed to revert memory deficits in a rat model of AD, strongly suggesting a prominent role of S1P signalling in neuroprotection against Aβ toxicity [33]. Subchronic treatment with fingolimod was also shown to decrease Ca^{2+} responsiveness of neurons to neurotoxic $A\beta_{42}O$, thus ameliorating the cognitive performance in transgenic APPswe/PS1E9 AD mice [34].

In this study, we investigated the molecular mechanisms underlying the protective effects of S1P from $A\beta_{42}O$ neurotoxicity in primary rat cortical neurons and human SH-SY5Y neuroblastoma cells. Our results indicate that S1P modulates NMDAR activation and the Ca^{2+} influx induced by $A\beta_{42}O$. Indeed, S1P transiently reduces the surface localization of the extrasynaptic GluN2B subunit of NMDARs through its endocytic internalization, occurring upon $S1P_1$ and $S1P_4$, and to a lower extent $S1P_3$ and $S1P_5$, activation, thus eliciting beneficial effects. Moreover, we provide important evidence for a protective effect of SK1 overexpression against $A\beta_{42}O$-mediated damage in neuronal cells.

Results

S1P reduces mitochondrial dysfunction, apoptosis and Ca^{2+} dyshomeostasis induced by toxic $A\beta_{42}O$

In this work, we exploited highly stable and well-characterized $A\beta_{42}$ oligomers ($A\beta_{42}O$) cross-reacting with the conformation-specific A11 antibody, referred to as prefibrillar oligomers [4] or A+ oligomers [35]. Previous evidence showed that these small and soluble aggregates cause massive neurological damage by impairing mitochondrial activity, inducing lactate dehydrogenase release and affecting Ca^{2+} homeostasis of neurons [4,35–37]. Using dot blot assays and confocal microscopy coupled to immunofluorescence with A11 antisera, these species were also found in AD brain lysates [4], as well as in AD brain specimens analysed with immunogold electron microscopy [38,39]. Here, we firstly compared the ability of $A\beta_{42}O$ to affect cytosolic Ca^{2+} homeostasis of human SH-SY5Y neuroblastoma cells with respect to monomeric $A\beta_{42}$, non-toxic prefibrillar $A\beta_{42}$ oligomers, that do

not react with the conformation-specific A11 antibody (A- $A\beta_{42}O$) and $A\beta_{42}$ fibrillar aggregates [35]. When $A\beta_{42}O$ were added to the culture medium for 15 min at a concentration of 3 μM (monomer equivalents), they caused an extensive influx of Ca^{2+} ions, whereas $A\beta_{42}$ fibrils slightly increased the cellular Ca^{2+} level. On the contrary, A- $A\beta_{42}O$ and the monomeric peptide ($A\beta_{42}M$) appeared to be innocuous (Fig. 1A). A dramatic increase in the Ca^{2+}-derived fluorescence was also observed in cells exposed to the ionophore ionomycin (Fig. 1A). Moreover, increasing concentrations (0.1, 0.3, 1, 3 and 10 μM, monomer equivalents) of $A\beta_{42}O$ triggered an overload of intracellular Ca^{2+} ions with a clear dose dependence up to 748 ± 27% employing 10 μM $A\beta_{42}O$ (Fig. 1B,C).

The neurotoxic effect of $A\beta_{42}O$ was also monitored by evaluating the reduction of 3-(4,5-dimethylthiazol-2-yl)-2,5 diphenyltetrazolium bromide (MTT) [4,40,41]. When increased concentrations of $A\beta_{42}O$ were added to the culture medium of SH-SY5Y cells for 24 h, the ability of cells to reduce MTT progressively decreased, reaching a value of 47 ± 5% at 10 μM $A\beta_{42}O$ with respect to untreated cells, taken as 100% (Fig. 1D). When the increase in the intracellular Ca^{2+} levels (Fig. 1C) was plotted versus the MTT reduction (Fig. 1D), a highly significant correlation between Ca^{2+} dyshomeostasis and $A\beta_{42}O$-induced mitochondrial dysfunction was found ($r = 0.88$, $P < 0.001$), (Fig. 1E). Consistently, 1 and 3 μM $A\beta_{42}O$ were found to cause apoptotic cell death, inducing caspase-3 cleavage measured by western blot analysis (Fig. 1F,G).

We then examined whether S1P could inhibit $A\beta_{42}O$ neurotoxicity in cultured cells. We first monitored the mitochondrial dysfunction by treating SH-SY5Y cells for 24 h with 3 μM $A\beta_{42}O$ in the absence or presence of S1P at concentrations ranging from 10 nM to 1 μM. The MTT reduction was significantly restored in the presence of 100 nM S1P, either pre-incubated or co-incubated with the oligomers (Fig. 2A), with a minor protective effect observed at both lower and higher concentrations, showing a bell-shaped S1P dependence (Fig. 2A). This reduced protection cannot be ascribed to inherent neurotoxicity of S1P *per se*, since the addition of 1 μM S1P to the culture medium in the absence of $A\beta_{42}O$ was not cytotoxic to SH-SY5Y cells (Fig. 2A). Accordingly, the activation of caspase-3 triggered by 3 μM $A\beta_{42}O$ added to the cell culture medium for 24 h was completely prevented by 100 nM S1P co-incubated with the oligomers, demonstrating a protective role of this sphingolipid against apoptotic cell death (Fig. 2B). As control, cells were also treated with S1P in the absence of $A\beta_{42}O$, without detecting any cytotoxic effect at the tested concentrations (Fig. 2B). On the basis of these results, 100 nM S1P was employed in all subsequent experiments.

We then investigated whether S1P was able to rescue the early Ca^{2+} dyshomeostasis induced by $A\beta_{42}O$ in SH-SY5Y cells. Thus, cells were treated with 3 μM $A\beta_{42}O$ for different lengths of time (5, 10 and 15 min), in the absence or presence of 100 nM S1P. Confocal microscopy analysis revealed that $A\beta_{42}O$ evoked a rapid and significant increase in the intracellular Ca^{2+} levels already after 5 min of treatment (by 250 ± 19% relative to untreated cells, taken as 100%), reaching higher levels at 10 and 15 min of treatment (by 265 ± 10% and 366 ± 15%, respectively) (Fig. 2C,D). The protective effect of S1P was significant at 15 min of treatment, with a reduction in Ca^{2+} dyshomeostasis by 167 ± 25% (Fig. 2C,D). Cells exposed to 100 nM S1P in the absence of $A\beta_{42}O$ for 15 min also showed a minor Ca^{2+} increase, in good agreement with the observed role of S1P in Ca^{2+} signals [42,43].

S1PR mediates the protective effect of S1P against $A\beta_{42}O$ neurotoxicity

We then examined whether the protective effect of S1P against $A\beta_{42}O$ toxicity was mediated by S1PR. Real-time PCR analysis of the mRNA expression levels of the S1PR family showed that all S1PRs were expressed in SH-SY5Y cells, with $S1P_3$ appearing to be the most abundant (Fig. 3A). In spite of their relative abundance, the treatment of cells with 3 μM $A\beta_{42}O$ for 24 h caused a significant down-regulation of the mRNA expression of $S1P_2$, $S1P_4$ and $S1P_5$, whereas $S1P_1$ and $S1P_3$ levels did not change (Fig. 3B).

Since all S1PRs, even not exclusively, couple with G_i proteins [44], we pre-treated the cells for 4 h with 200 $ng \cdot mL^{-1}$ Pertussis toxin (PTX), a specific inhibitor of G_i/G_o proteins [45], to investigate the involvement of S1PR in mediating the S1P neuroprotective effect in SH-SY5Y cells. The beneficial effect of S1P on $A\beta_{42}O$-induced Ca^{2+} entry was completely lost in the presence of PTX (Fig. 3C,D), demonstrating that the S1P action was G_i dependent.

Thus, the involvement of S1PR in mediating the protective effect of S1P against $A\beta_{42}O$ toxicity was evaluated with specific S1PR antagonists. To this aim, SH-SY5Y cells were pre-incubated with specific antagonists of $S1P_1$, $S1P_2$, $S1P_3$ or $S1P_4$ for 30 min, and then treated with 3 μM $A\beta_{42}O$ for 15 min, in the absence or presence of 100 nM S1P. The ability of S1P to reduce $A\beta_{42}O$-induced Ca^{2+} influx was partially impaired in the presence of the $S1P_1$ or $S1P_4$ selective antagonists W146 [46] and CYM50358 [47] respectively (light green bars in Fig. 4A,B). The inhibition of $S1P_3$

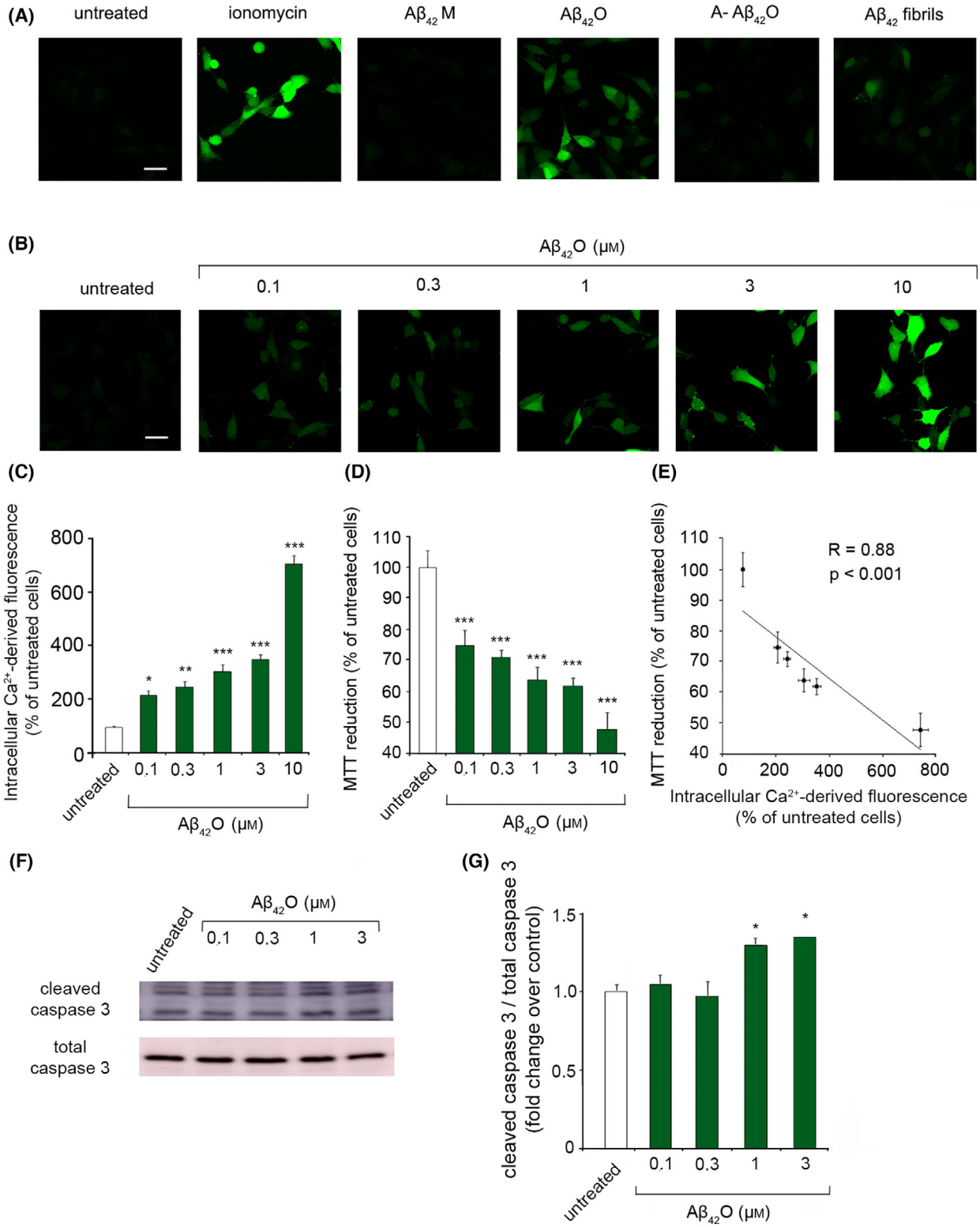

by its specific antagonist CAY10444 partially reduced S1P protection, whereas that of of $S1P_2$ by its specific antagonist JTE013 did not produce any detectable effect (Fig. 4A,B). The functional blockade of both $S1P_1$ and $S1P_3$ with the antagonist VPC23019 confirmed the role of such receptors in S1P-mediated

Fig. 1. (A) Representative confocal microscope images showing the Ca^{2+}-derived fluorescence in SH-SY5Y cells treated for 15 min with 1 μM ionomycin, or with the indicated $A\beta_{42}$ species at 3 μM and then loaded with the Fluo-4 AM probe. Untreated cells are also shown. (B) Representative confocal microscope images showing the Ca^{2+}-derived fluorescence in SH-SY5Y cells treated for 15 min with increasing concentrations (0.1, 0.3, 1, 3 and 10 μM) of $A\beta_{42}O$ and then loaded with the Fluo-4 AM probe. Untreated cells are also shown. (C) Semi-quantitative analysis of the intracellular Ca^{2+}-derived fluorescence referring to panel (B). (D) MTT reduction in SH-SY5Y cells treated for 24 h with increasing concentrations (0.1, 0.3, 1, 3 and 10 μM) of $A\beta_{42}O$. (E) MTT reduction values reported in panel (D) plotted against the Ca^{2+}-derived fluorescence reported in panel (C) at the corresponding concentrations. In all panels, data are expressed as the percentage of the value for untreated cells. (F) Representative western blotting analysis of cell lysates from SH-SY5Y cells treated for 24 h with increasing concentrations (0.1, 0.3, 1 and 3 μM) of $A\beta_{42}O$. Caspase-3 cleavage was measured in total cell lysate by using a specific anti-caspase-3 antibody. (G) Band intensity of western blotting in (F) was quantified by densitometric analysis and normalized to the expression of the total caspase-3. Data are expressed as fold increase relative to the untreated sample, set as 1. Experimental errors are SEM ($n = 3$). A total of 60–100 cells (B, C), 200 000–250 000 cells (D) and 15 μg of cell lysates (F, G) were analysed per condition. Samples were analysed by one-way ANOVA followed by Bonferroni's multiple-comparison test relative to untreated cells (*$P < 0.05$, **$P < 0.01$, ***$P < 0.001$) in panels (C) and (D), or by one-way ANOVA followed by Bonferroni's *post hoc* test relative to untreated cells (*$P < 0.05$) in panel (G). Scale bars, 30 μM.

neuroprotection (Fig. 4A,B). S1PR antagonists did not affect the Ca^{2+} influx triggered by 3 μM $A\beta_{42}O$ in the absence of 100 nM S1P (Fig. 4A,B). Accordingly, the MTT test revealed that S1P protection was markedly reduced by the blockade of $S1P_1$ and partially prevented by $S1P_3$ and $S1P_4$ antagonists, but fully reduced by the combined antagonism of all three receptors (Fig. 4C). Most studies that validate the S1PR-blocking effects of S1P antagonists used concentrations equal to or lower than 1 μM, while evidence of non-specificity at higher concentrations was found [48]. Thus, a slight inhibition of all S1PRs by a selective S1P antagonist cannot be ruled out in our experimental conditions. In addition, a cross-talk between different S1PR signalling pathways could cause a minor response of other S1PR when a single S1PR was inhibited.

We next exploited the potent and high-selective $S1P_1$ and $S1P_4$ agonists SEW2871 and CYM50308, respectively, to further confirm the role of these receptors in S1P axis [49,50].

Thus, $A\beta_{42}O$ were added to the SH-SY5Y cell culture medium at 3 μM for 15 min in the presence or absence of S1PR agonists at 1 μM. We observed a partial and complete reduction in the early Ca^{2+} dyshomeostasis evoked by $A\beta_{42}O$ when the two agonists were used separately and together, respectively (Fig. 4D,E).

To validate our results with a different method, the specific involvement of individual S1PR in the protective effect of S1P against $A\beta_{42}O$ toxicity was evaluated by RNA interference. Indeed, SH-SY5Y cells were transfected with a siRNA-negative control or with siRNAs against $S1P_1$, $S1P_2$, $S1P_3$, $S1P_4$ and $S1P_5$, and then treated for 15 min with 3 μM $A\beta_{42}O$ in the absence or presence of 100 nM S1P. $A\beta_{42}O$ evoked a significant Ca^{2+} entry in cells transfected with the control siRNA (370 ± 27% relative to control cells), which was significantly reduced by 100 nM S1P (by 195 ± 36%). Notably, the S1P-mediated reduction was remarkably lower in cells pre-treated with siRNAs. The most effective was the siRNA against $S1P_1$, followed by the siRNA against $S1P_4$, and then $S1P_3$ and $S1P_5$, whereas the silencing of $S1P_2$ did not impair the beneficial effect of S1P (Fig. 5A,B). Accordingly, S1P beneficial action was completely lost in cells transfected with a combination of all siRNAs (Fig. 5A,B). Overall, these data indicate that S1P protection against harmful $A\beta_{42}O$ involves $S1P_1$, $S1P_3$, $S1P_4$ and $S1P_5$.

S1P rescues Ca^{2+} dyshomeostasis by modulating NMDARs exposure on neuronal membrane

An increasing body of evidence strongly indicates that $A\beta_{42}O$ evoke a massive Ca^{2+} influx through the activation of NMDARs, particularly at the early stages of the observed Ca^{2+} uptake [12,17,18,51]. We, therefore, assessed whether S1P prevents neuronal Ca^{2+} responsiveness by modulating NMDAR activity. Pre-treatment of SH-SY5Y cells with 10 μM mem, a low-affinity NMDAR antagonist, significantly reduced the rapid Ca^{2+} increase evoked by 3 μM $A\beta_{42}O$ for 15 min (by 196 ± 48%), confirming a crucial role for NMDARs in the early neuronal Ca^{2+} dysregulation (Fig. 6A,B). Similarly, the silencing of the 2B subunit of NMDARs (GluN2B) by its specific siRNA in SH-SY5Y cells also resulted in a significant reduction in intracellular Ca^{2+} levels (by 196 ± 31%) induced by 3 μM $A\beta_{42}O$ for 15 min, compared with cells transfected with a negative control siRNA and then treated with the same species (Fig. 6A,B).

When NMDARs were activated in primary rat cortical neurons with their specific agonist NMDA at 1 mM for 15 min, we observed a dramatic increase in

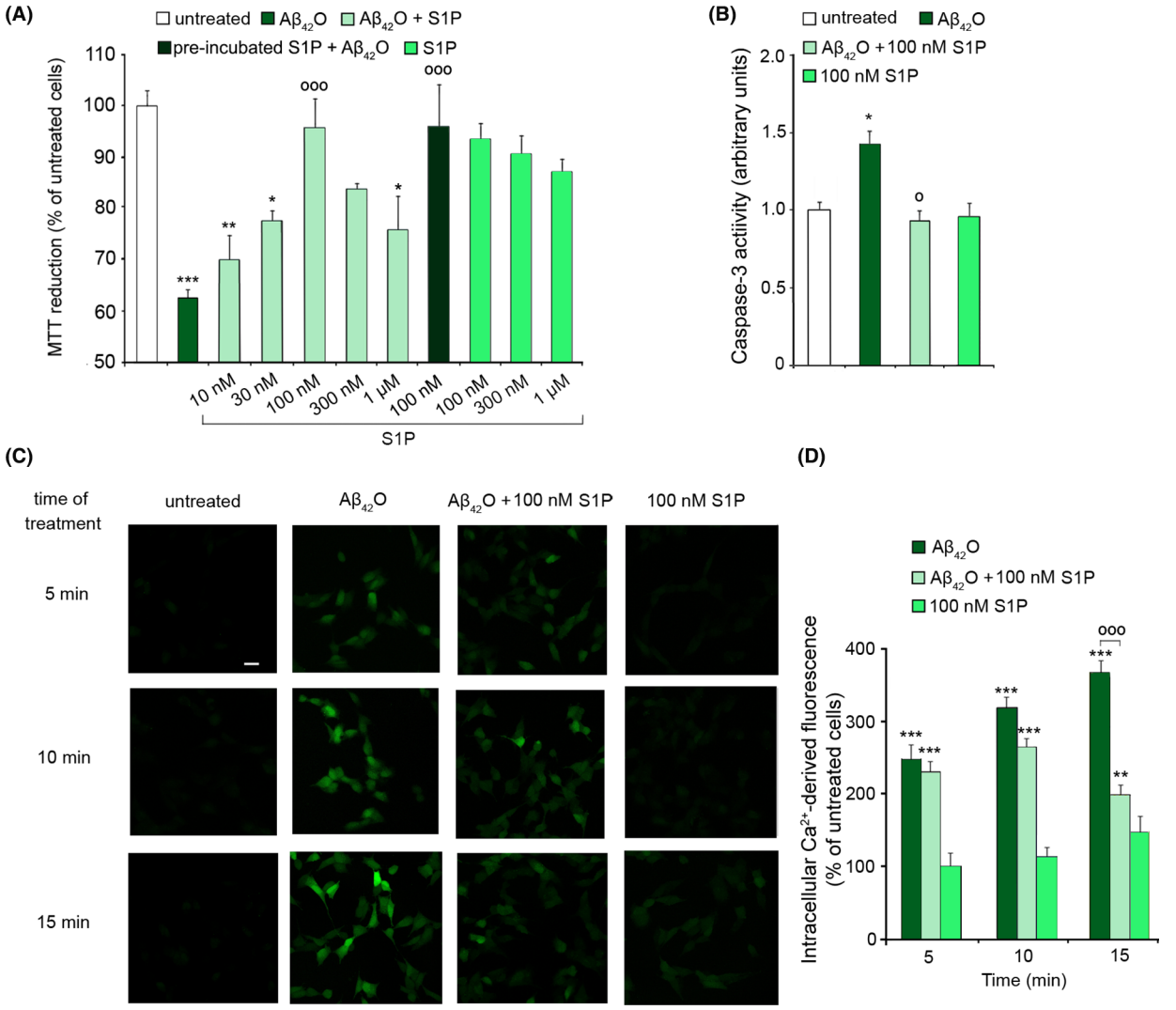

Fig. 2. (A) MTT reduction in SH-SY5Y cells treated for 24 h with 3 μM $A\beta_{42}O$ in the absence or presence of a co-incubation with increasing concentrations (10, 30, 100, 300 nM and 1 μM) of S1P. Cells were also pre-incubated with 100 nM S1P for 15 min and then treated with 3 μM $A\beta_{42}O$. S1P alone at increasing concentrations (100, 300 nM and 1 μM) was also tested as a control. Data are expressed as the percentage of the value for untreated cells. (B) Fluorimetric analysis of the caspase-3 activity in SH-SY5Y treated for 24 h with 3 μM $A\beta_{42}O$ in the absence or presence of 100 nM S1P. Cells were also treated with 100 nM S1P alone as a control. Data are expressed as fold increase relative to the untreated sample, set as 1. (C) Representative confocal microscope images showing the Ca^{2+}-derived fluorescence in SH-SY5Y cells treated for 5, 10 and 15 min with 3 μM $A\beta_{42}O$ in the absence or presence of 100 nM S1P and then loaded with the Fluo-4 AM probe. Untreated cells and cells treated with 100 nM S1P alone are also shown. (D) Semi-quantitative analysis of the intracellular Ca^{2+}-derived fluorescence referring to panel (C). Data are expressed as the percentage of the value for untreated cells. Experimental errors are SEM ($n = 4$ in panel (A) and $n = 3$ in panels (B–D). A total of 200 000–250 000 cells (A), 15 μg of cell lysates (B) and 60–100 cells (C, D) were analysed per condition. Samples were analysed by one-way ANOVA followed by Bonferroni's multiple-comparison test relative to untreated cells (*$P < 0.05$, **$P < 0.01$, ***$P < 0.001$) and to cells treated with $A\beta_{42}O$ (°°°$P < 0.001$) in panels (A) and (D), or by Student's t test relative to untreated cells (*$P < 0.05$) and to cells treated with $A\beta_{42}O$ in the absence of S1P (°$P < 0.05$), in panel (B). Scale bar, 30 μM.

intracellular calcium (by 745 ± 46%) with respect to untreated cells, which was slightly higher than that observed upon treatment with 3 μM $A\beta_{42}O$ (566 ± 66%) (Fig. 6C,D). Notably, the presence of 100 nM S1P significantly reduced the Ca^{2+} influx induced by both NMDA (by 356 ± 111%) and $A\beta_{42}O$ (by 423 ± 72%) respectively (Fig. 6C,D). The presence of the $S1P_1$ antagonist W146 and, to a lesser extent, $S1P_3$ and $S1P_4$ antagonists CYM50358 and CAY10444, partially prevented the beneficial effect of

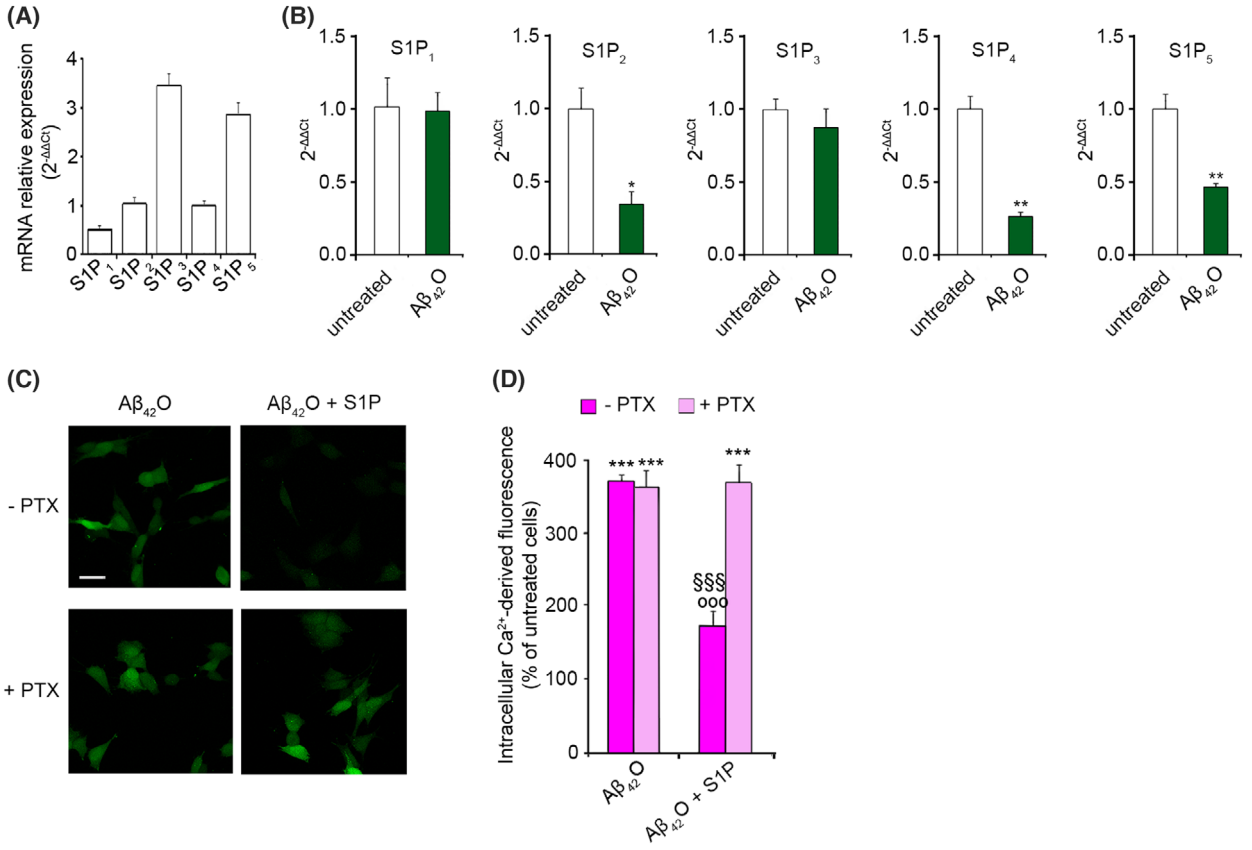

Fig. 3. (A) Quantitative mRNA analysis of $S1P_{1–5}$ in SH-SY5Y cells. Data are expressed according to the $2^{-\Delta\Delta Ct}$ method, using $S1P_4$ as calibrator. (B) Quantitative mRNA analysis of $S1P_{1–5}$ in SH-SY5Y cells treated for 24 h with 3 μM $Aβ_{42}O$. S1PR mRNA quantitation was based on the $2^{-\Delta\Delta Ct}$ method, using individual S1PR subtype of the unchallenged specimen as calibrator. (C) Representative confocal microscope images showing the Ca^{2+}-derived fluorescence in SH-SY5Y cells treated for 15 min with 3 μM $Aβ_{42}O$ in the absence or presence of 100 nM S1P, following 4 h of pre-treatment with 200 ng·mL^{-1} PTX. Cells were then loaded with the Fluo-4 AM probe. (D) Semi-quantitative analysis of the intracellular Ca^{2+}-derived fluorescence referring to panel (C). Data are expressed as the percentage of the value for untreated cells. Experimental errors are SEM ($n = 3$). A total of 1–2 μg of RNA (A, B) and 60–100 cells (C, D) were analysed per condition. Samples were analysed by Student's t test relative to untreated cells (*$P < 0.05$, **$P < 0.01$) in panel (B), or by one-way ANOVA followed by Bonferroni's multiple-comparison test relative to untreated cells (***$P < 0.001$), to cells treated with $Aβ_{42}O$ in the absence of S1P and PTX (°°°$P < 0.001$) and to cells treated with $Aβ_{42}O$ + S1P in the presence of PTX (§§§$P < 0.001$) in panel (D). Scale bar, 30 μM.

S1P (Fig. 6C,D). These results indicate that S1P signalling helps the maintenance of Ca^{2+} homeostasis in NMDA-stimulated primary rat cortical neurons by blocking the Ca^{2+} influx occurring via NMDARs (Fig. 6A–D).

Then, we investigated whether the protective effect of S1P against $Aβ_{42}O$ could be mediated by relocation of extrasynaptic GluN2B-containing NMDARs [51,52]. Thus, the distribution of the NMDAR subunit GluN2B on the neuronal membrane of SH-SY5Y cells was determined after transfecting cells with the control siRNA or with siRNA against the S1P receptors and then adding $Aβ_{42}O$ to the culture medium, in the absence or presence of S1P (Fig. 7A,B). We observed that 100 nM S1P and 100 nM S1P with 3 μM $Aβ_{42}O$ significantly reduced the membrane exposure of GluN2B (by 49 ± 9% and 53 ± 8%, respectively) in cells transfected with control siRNA, whereas 3 μM $Aβ_{42}O$ did not evoke any appreciable mobilization of the subunit (Fig. 7A,B). Consistently, the pre-treatment of SH-SY5Y cells with 50 μM dynasore (dyn), a cell-permeable-specific inhibitor of dynamin, totally prevented the clathrin-mediated endocytosis of NMDARs (Fig. 7A,B). In such conditions, an overall inhibition of the physiological recycling of the NMDARs should be speculated, as the percentage of exposed GluN2B was slightly higher with respect to untreated cells. Notably, a reduced internalization of GluN2B was observed in cells pre-treated with siRNA against $S1P_1$, $S1P_4$ and, to a minor extent, $S1P_3$ and

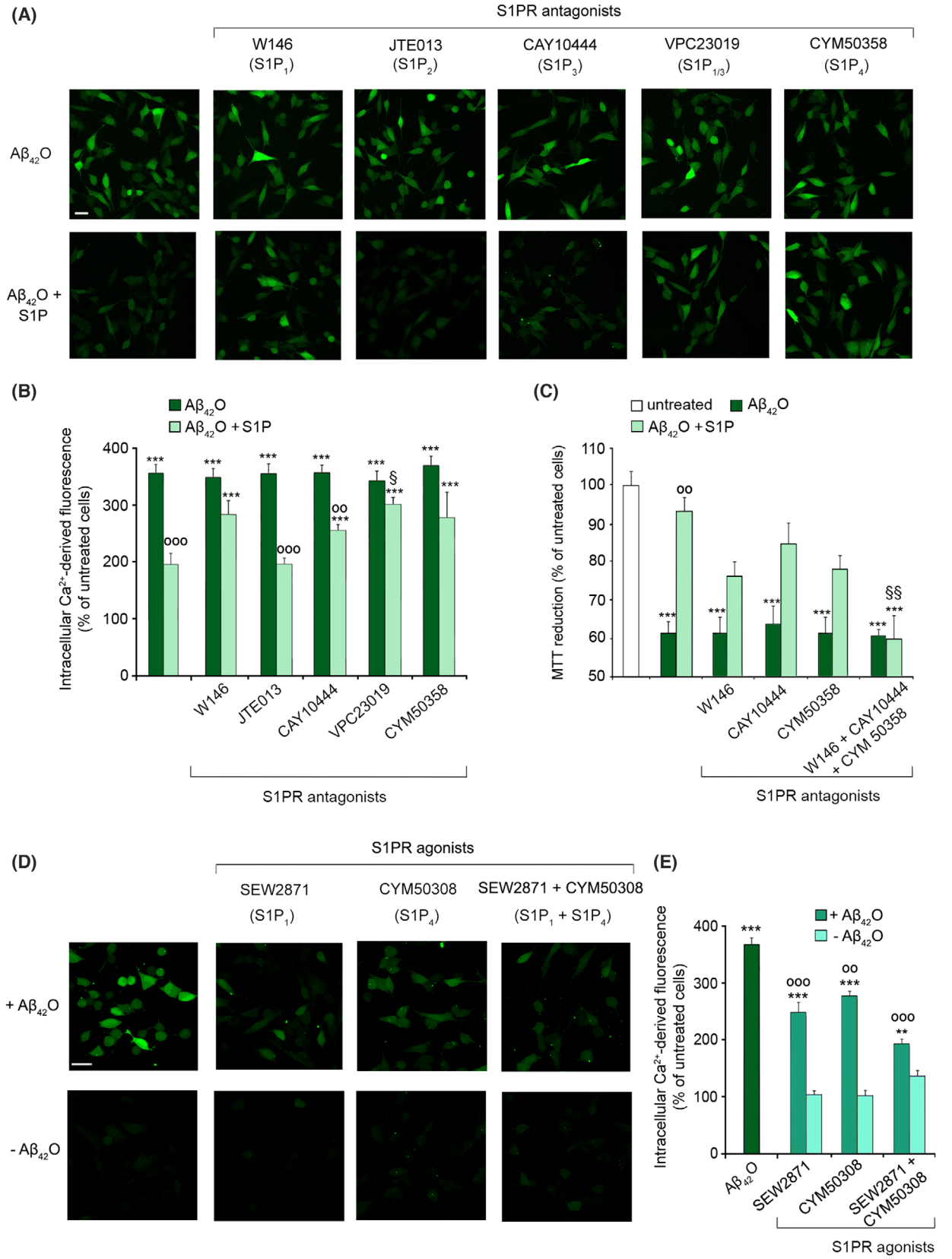

Fig. 4. (A) Representative confocal microscope images showing the Ca^{2+}-derived fluorescence in SH-SY5Y cells treated for 15 min with 3 μM $A\beta_{42}O$ in the absence or presence of 100 nM S1P, following 30 min of pre-treatment with the S1PR antagonists W146 ($S1P_1$) at 10 μM, JTE013 ($S1P_2$) at 1 μM, CAY10444 ($S1P_3$) at 5 μM, VPC23019 ($S1P_1$ and $S1P_3$) at 1 μM and CYM50358 ($S1P_4$) at 1 μM. Cells were then loaded with the Fluo-4 AM probe. (B) Semi-quantitative analysis of the intracellular Ca^{2+}-derived fluorescence referring to panel (A). (C) MTT reduction in SH-SY5Y cells treated for 24h with 3 μM $A\beta_{42}O$ in the absence or presence of 100 nM S1P, following 30 min of pre-treatment with W146 at 10 μM, CAY10444 at 5 μM, CYM50358 at 1 μM and with all the antagonists together at the previously reported concentrations. (D) Representative confocal microscope images showing the Ca^{2+}-derived fluorescence in SH-SY5Y cells treated for 15 min with 3 μM $A\beta_{42}O$ in the absence or presence of 100 nM S1P or the S1PR agonists SEW2871 ($S1P_1$) at 10 μM and CYM50308 ($S1P_4$) at 1 μM, and both agonists together at the previously reported concentrations. Cells were then loaded with the Fluo-4 AM probe. (E) Semi-quantitative analysis of the intracellular Ca^{2+}-derived fluorescence referring to panel (D). In all panels, data are expressed as the percentage of the value for untreated cells. A total of 80–120 cells (A–B, D–E) and 200 000–250 000 cells (C) were analysed per condition. Experimental errors are SEM ($n = 3$). Samples were analysed by one-way ANOVA followed by Bonferroni's multiple-comparison test relative to untreated cells (**$P < 0.01$, ***$P < 0.001$), to cells treated with $A\beta_{42}O$ alone (°°$P < 0.01$, °°°$P < 0.001$), and to cells treated with $A\beta_{42}O$ + S1P in the absence of S1PR antagonists (§$P < 0.05$, §§$P < 0.01$). Scale bars, 30 μM.

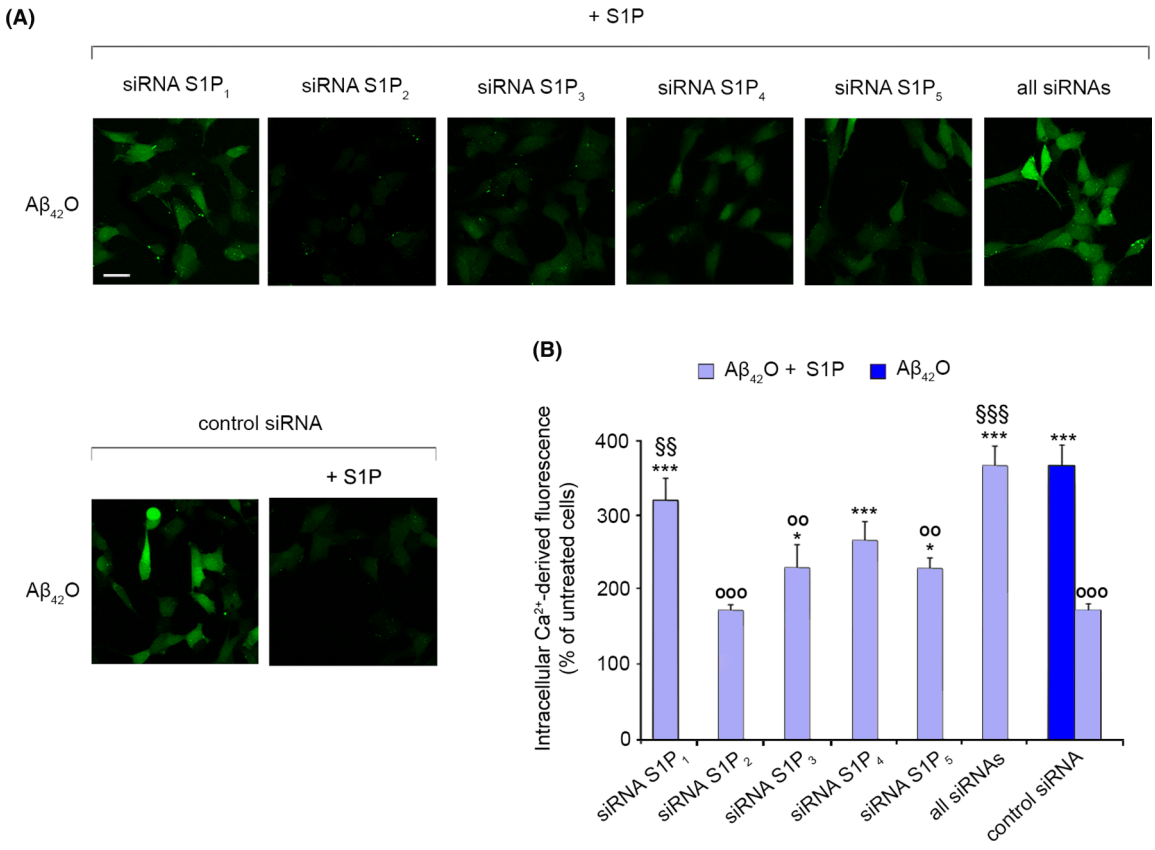

Fig. 5. (A) Representative confocal microscope images showing the Ca^{2+}-derived fluorescence in SH-SY5Y cells pre-transfected with siRNA against $S1P_1$, $S1P_2$, $S1P_3$, $S1P_4$ and $S1P_5$ receptors and with all the analysed siRNAs or control siRNA, and then treated for 15 min with 3 μM $A\beta_{42}O$ in the absence or presence of 100 nM S1P. Cells were then loaded with the Fluo-4 AM probe. (B) Semi-quantitative analysis of the intracellular Ca^{2+}-derived fluorescence referring to panel (A). Data are expressed as the percentage of the value for untreated cells. Experimental errors are SEM ($n = 3$). A total of 80–100 cells were analysed per condition. Samples were analysed by one-way ANOVA followed by Bonferroni's multiple-comparison test relative to untreated cells pre-transfected with control siRNA (*$P < 0.05$, ***$P < 0.001$), to cells pre-transfected with control siRNA and treated with $A\beta_{42}O$ alone (°°$P < 0.01$, °°°$P < 0.001$), and to cells pre-transfected with control siRNA and then treated with $A\beta_{42}O$ + S1P (§§$P < 0.01$, §§§$P < 0.001$). Scale bar, 30 μM.

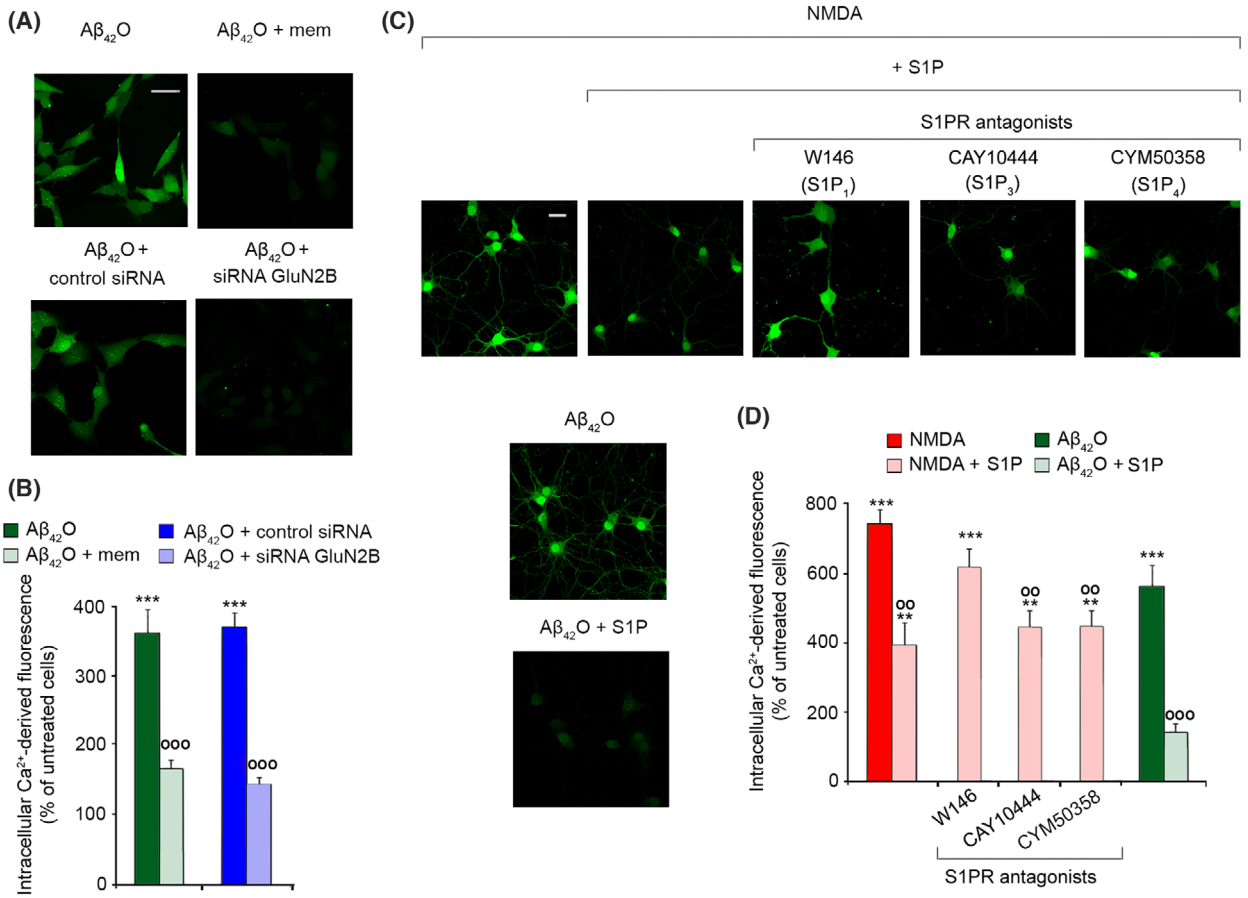

Fig. 6. (A) Representative confocal microscope images showing the Ca^{2+}-derived fluorescence in SH-SY5Y cells treated for 15 min with 3 μM $A\beta_{42}O$ in the absence or presence of a 60 min pre-treatment with 10 μM mem (upper panels), or in the presence of a pre-transfection with control siRNA and with siRNA against GluN2B subunit (lower panels). Cells were then loaded with the Fluo-4 AM probe. (B) Semi-quantitative analysis of the intracellular Ca^{2+}-derived fluorescence referring to panel (A). Data are expressed as the percentage of the value for untreated not-tranfected cells, or untreated cells pre-transfected with control siRNA. (C) Representative confocal microscope images showing the Ca^{2+}-derived fluorescence in primary rat cortical neurons treated with 1 mM NMDA in the absence or presence of 100 nM S1P, following 30 min of pre-treatment with the S1PR antagonists W146 ($S1P_1$) at 10 μM, CAY10444 ($S1P_3$) at 5 μM and CYM50358 ($S1P_4$) at 1 μM. Cells were also treated with 3 μM $A\beta_{42}O$ in the absence or presence of 100 nM S1P, and then loaded with the Fluo-4 AM probe. (D) Semi-quantitative analysis of the intracellular Ca^{2+}-derived fluorescence referring to panel (C). Data are expressed as the percentage of the value for untreated cells. Experimental errors are SEM ($n = 3$). A total of 60–100 cells (A, B) and 80–120 cells (C, D) were analysed per condition. Samples were analysed by one-way ANOVA followed by Bonferroni's multiple-comparison test relative to untreated cells (**$P < 0.01$, ***$P < 0.001$), to cells treated with $A\beta_{42}O$ in the absence of mem, or in the presence of the control siRNA ($^{\circ\circ\circ}P < 0.001$) in panel (B), and to cells treated with NMDA or $A\beta_{42}O$ alone ($^{\circ\circ}P < 0.01$, $^{\circ\circ\circ}P < 0.001$) in panel (D). Scale bars, 30 μM (A) and 20 μM (C).

Fig. 7. (A) Representative confocal microscope images showing the immunostaining of GluN2B subunit of NMDARs in SH-SY5Y cells that were either not-transfected, pre-transfected with control siRNA, or pre-transfected with siRNA against $S1P_1$, $S1P_2$, $S1P_3$, $S1P_4$ and $S1P_5$ receptors and with all the five siRNAs, and then treated with 3 μM $A\beta_{42}O$ for 15 min in the absence or presence of 100 nM S1P, following 30 min of pre-treatment with 50 μM dyn. (B) Semi-quantitative analysis of the number of fluorescent puncta on the membrane surface of SH-SY5Y cells referring to panel (A). Data are expressed as the percentage of the value for untreated cells pre-transfected with control siRNA. (C) Representative confocal microscope images showing the Ca^{2+}-derived fluorescence in SH-SY5Y cells treated for 15 min with 3 μM $A\beta_{42}O$, or with 1 mM NMDA, in the absence or presence of 100 nM S1P, and following 30 min of pre-treatment with 50 μM dyn. Cells were then loaded with the Fluo-4 AM probe. (D) Semi-quantitative analysis of the intracellular Ca^{2+}-derived fluorescence referring to panel (C). Data are expressed as the percentage of the value for untreated cells. Experimental errors are SEM ($n = 3$). A total of 80–120 cells (A, B) and 60–100 cells (C, D) were analysed per condition. Samples were analysed by one-way ANOVA followed by Bonferroni's multiple-comparison test relative to untreated cells (*$P < 0.05$, **$P < 0.01$, ***$P < 0.001$), to cells transfected with control siRNA and then treated with $A\beta_{42}O$ + S1P ($^{\S}P < 0.05$, $^{\S\S}P < 0.01$, $^{\S\S\S}P < 0.001$) in panel (B), and to cells treated with $A\beta_{42}O$ + S1P, or NMDA + S1P in the absence of dyn ($^{\S\S\S}P < 0.001$) in panel (D). Scale bars, 10 μM (A) and 30 μM (C).

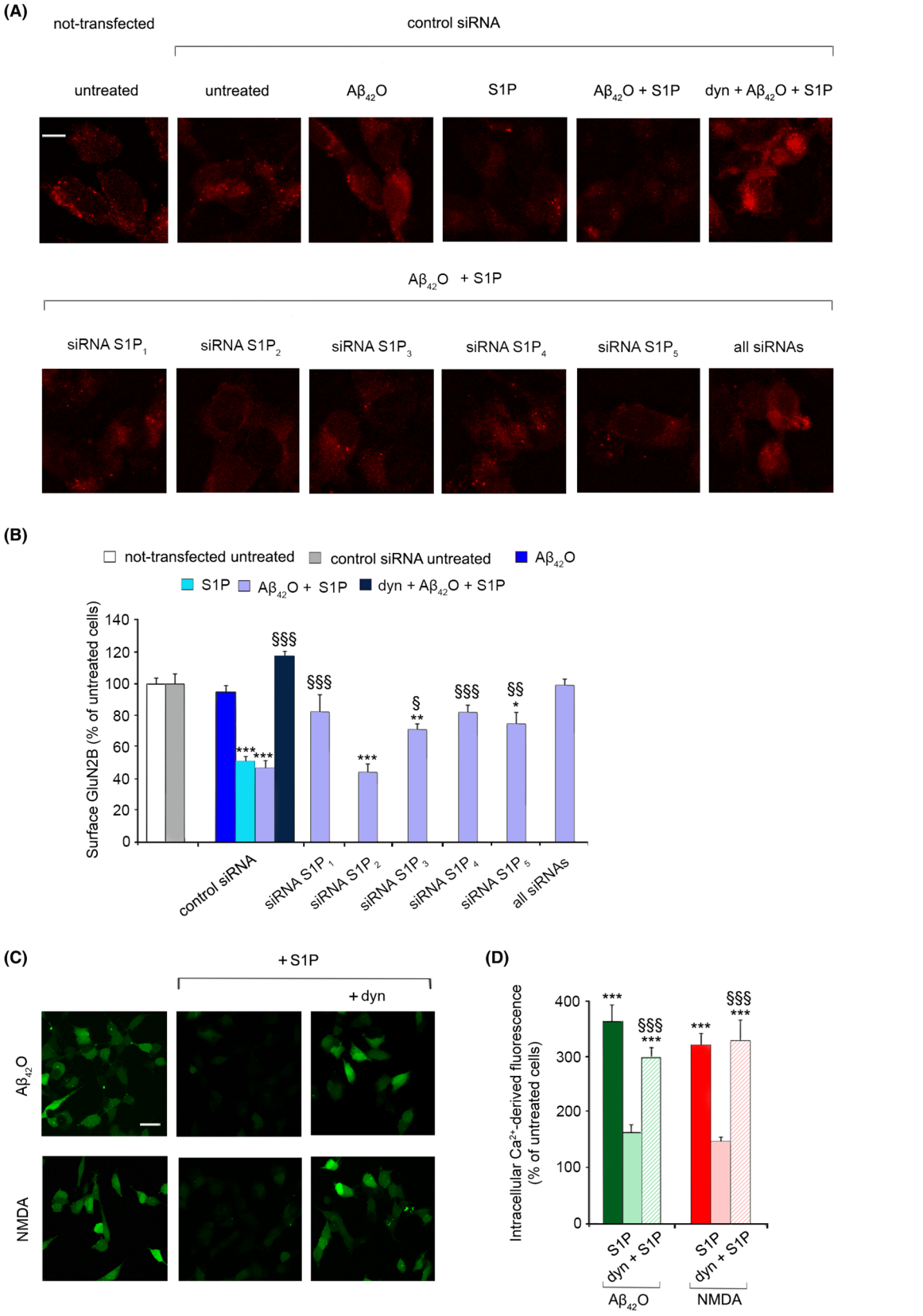
(A)
not-transfected
control siRNA
untreated
untreated
Aβ42O
S1P
Aβ42O + S1P
dyn + Aβ42O + S1P
Aβ42O + S1P
siRNA S1P1
siRNA S1P2
siRNA S1P3
siRNA S1P4
siRNA S1P5
all siRNAs
(B)
not-transfected untreated
control siRNA untreated
Aβ42O
S1P
Aβ42O + S1P
dyn + Aβ42O + S1P
Surface GluN2B (% of untreated cells)
control siRNA
siRNA S1P1
siRNA S1P2
siRNA S1P3
siRNA S1P4
siRNA S1P5
all siRNAs
(C)
+S1P
+dyn
Aβ42O
NMDA
(D)
Intracellular Ca2+-derived fluorescence (% of untreated cells)
S1P
dyn + S1P
Aβ42O
NMDA

$S1P_5$, whereas the silencing of $S1P_2$ did not reduce the effect of S1P (Fig. 7A,B). Consistently, the simultaneous silencing of all S1PRs completely abolished GluN2B internalization (Fig. 7A,B).

According to data obtained in primary rat cortical neurons, NMDA induced a significant increase in intracellular calcium (by 320 ± 18% relative to untreated cells) in SH-SY5Y cells, comparable to that observed when cells were treated with 3 μM $A\beta_{42}O$ (by 362 ± 37%) (Fig. 7C,D). The incubation with 100 nM S1P significantly reduced the Ca^{2+} influx evoked by both NMDA and $A\beta_{42}O$ (Fig. 7C,D), strengthening S1P role in the membrane depletion of extrasynaptic GluN2B-containing NMDARs.

Notably, 50 μM dyn completely abolished the protective effect of S1P against the massive increase in intracellular Ca^{2+} evoked by 3 μM $A\beta_{42}O$ or 1 mM NMDA (Fig. 7C,D). Taken together, these results indicate that the early Ca^{2+} dysregulation induced by $A\beta_{42}O$ is mitigated by S1P through the dynamin-dependent endocytosis of GluN2B-containing NMDARs, occurring upon the activation of S1P receptors.

Endogenous S1P protects against harmful $A\beta_{42}O$

The ability of $A\beta_{42}O$ to modulate the mRNA expression levels of SK1, SK2 and Spns2 involved in S1P signalling axis was also evaluated in SH-SY5Y cells exposed to 3 μM $A\beta_{42}O$ for 24 h. A significant down-regulation of SK1 and SK2 expression was found, indicating an impairment of the S1P signalling evoked by $A\beta_{42}O$ (Fig. 8A). $A\beta_{42}O$ also induced a significant decrease in Spns2 expression (Fig. 8A). The mRNA expression levels of SPL and SPP1 were diminished, whereas those of SPP2 were not significantly altered by $A\beta_{42}O$ (Fig. 8A). The reduction in SK1, SK2 and Spns2 expression elicited by $A\beta_{42}O$ was also confirmed at the protein level by western blotting analysis (Fig. 8 B,C). Thus, in line with literature data, the $A\beta_{42}O$ toxic effect envisages the alteration of the metabolism and signalling of S1P [53].

To investigate whether the sustained endogenous S1P production could overcome the $A\beta_{42}O$ detrimental effect, we transiently overexpressed Flag-tagged SK1 in SH-SY5Y (SK1+) cells, since SK1 is the isoform responsible for the generation of the S1P pool involved in the "inside-out signalling" [25]. SK1+ cells displayed a significant overexpression of SK1 protein with respect to cells transfected with either control empty vector (pcDNA) or lipofectamine (vehicle), as shown using western blotting analysis (Fig. 9A). The intracellular Ca^{2+} increase induced by 3 μM $A\beta_{42}O$ was significantly lower in SK1+ cells (195 ± 35%) than in cells transfected with the empty

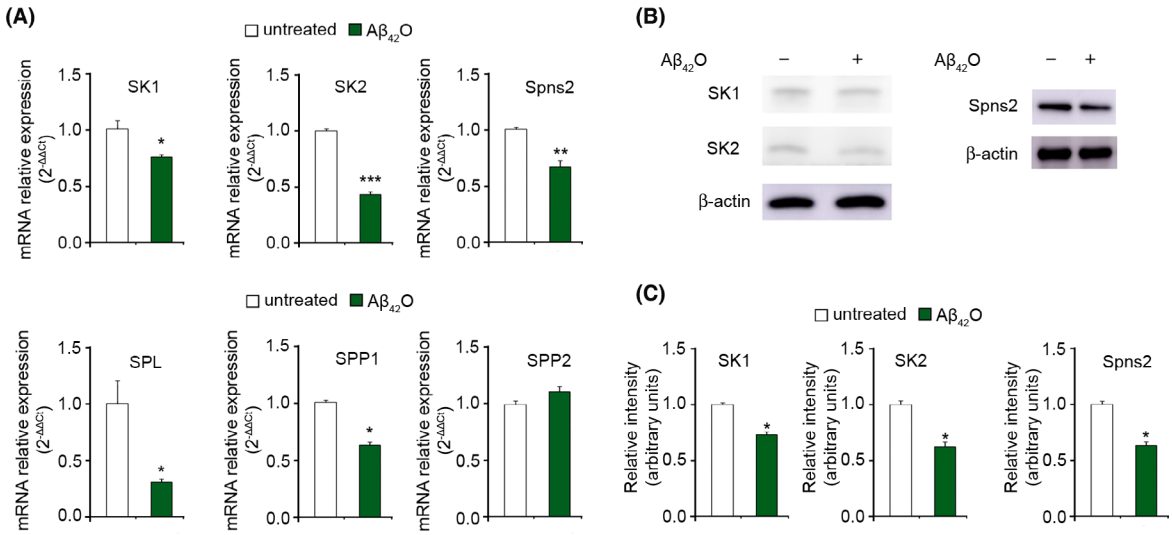

Fig. 8. (A) Quantitative mRNA analysis of SK1, SK2, Spns2, SPL, SPP1 and SPP2 performed by a real-time polymerase chain reaction in total RNA extracted from SH-SY5Y cells treated with 3 μM $A\beta_{42}O$ for 24 h. S1P metabolism enzymes and Spns2 mRNA quantitation was based on the $2^{-\Delta\Delta Ct}$ method, using individual enzyme or Spns2 of the unchallenged specimen as calibrator. (B) Western blotting analysis of SK1, SK2 and Spns2 expression in SH-SY5Y cells treated with 3 μM. $A\beta_{42}O$ for 24 h. A blot representative of three independent experiments is shown. (C) Band intensity of western blotting shown in panel (B), quantified by densitometric analysis and normalized to the expression of β-actin. Data are expressed as fold increase relative to the untreated specimen, set as 1. Experimental errors are SEM ($n = 3$). A total of 1–2 μg of RNA (A) and 15 μg of cell lysates (B, C) were analysed per condition. Samples were analysed by Student's t test relative to untreated cells (*$P < 0.05$, **$P < 0.01$, ***$P < 0.001$).

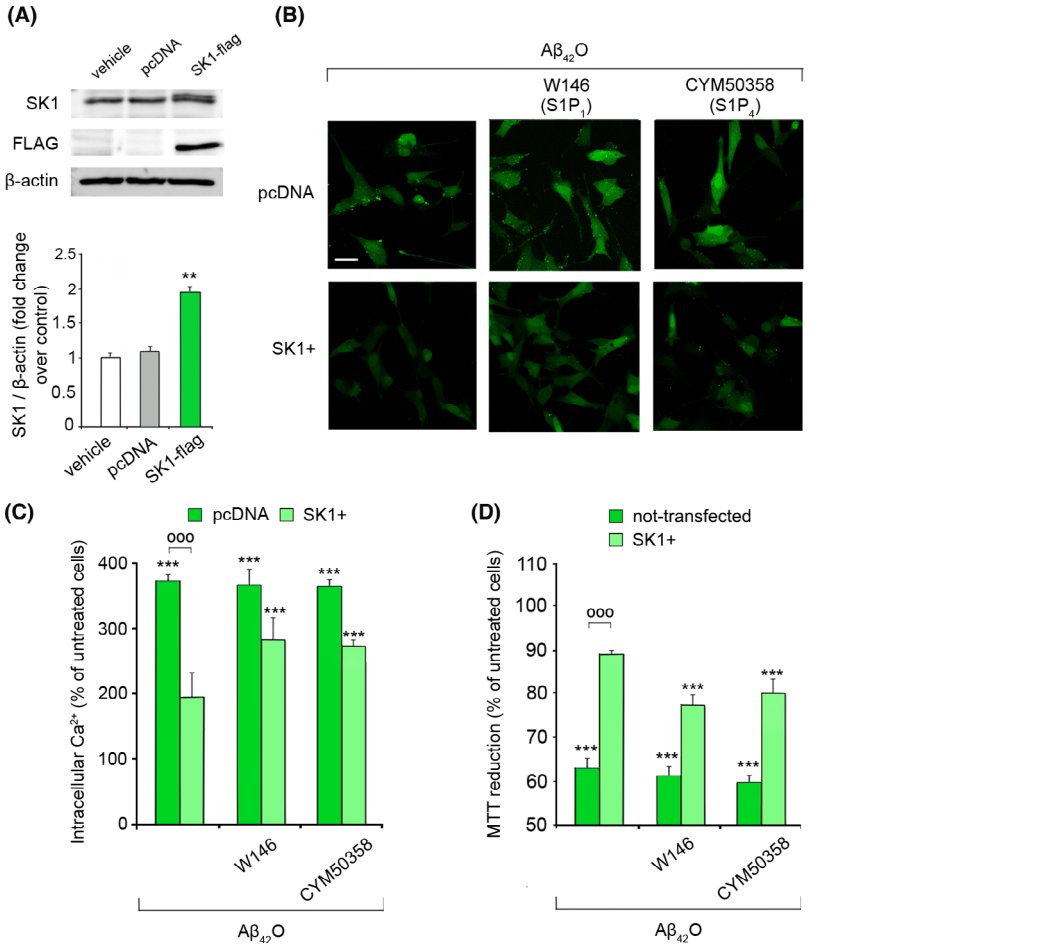

Fig. 9. (A) Representative western blotting analysis of SK1-flag in SH-SY5Y cells. Cells were transiently transfected with pcDNA3-human SK1-flag plasmid or pcDNA3 empty vector (pcDNA), or only with the transfection reagent (vehicle). The histogram shows the band intensities, quantified by densitometric analysis and normalized to the expression of β-actin. Data are expressed as fold increase relative to cells transfected with vehicle, set as 1. (B) Representative confocal microscope images showing the Ca^{2+}-derived fluorescence in SH-SY5Y cells pre-transfected with pcDNA or SK1-Flag plasmid (SK1+), and then treated for 15 min with 3 μM $A\beta_{42}O$, following 30 min of pre-treatment with the S1PR antagonists W146 ($S1P_1$) at 10 μM and CYM50358 ($S1P_4$) at 1 μM. Cells were then loaded with the Fluo-4 AM probe. (C) Semi-quantitative analysis of the intracellular Ca^{2+}-derived fluorescence referring to panel (B). Data are expressed as the percentage of the value for untreated cells pre-transfected with the respective plasmid. (D) MTT reduction in not-transfected SH-SY5Y cells, or pre-transfected with SK1-Flag plasmid (SK1+), and then treated for 24 h with 3 μM $A\beta_{42}O$ following 30 min of pre-treatment with the S1PR antagonists W146 at 10 μM and CYM50358 at 1 μM. Data are expressed as the percentage of the value for untreated not-transfected cells (vivid green), or untreated cells pre-transfected with pcDNA (pale green). Experimental errors are SEM (n = 3). 15 μg of cell lysates (A), 80–120 cells (B, C) and 200 000–250 000 cells (D) were analysed per condition. Samples were analysed by Student's *t* test relative to untreated cells in panel (A) (**$P < 0.01$), or by one-way ANOVA followed by Bonferroni's multiple-comparison test relative to untreated cells (**$P < 0.01$, ***$P < 0.001$), and to pcDNA transfected or not-transfected cells with the same treatment (°°°$P < 0.001$) in panels (C) and (D). Scale bars, 30 μM.

vector (372 ± 9%) (Fig. 9B,C), which is in good agreement with the above-reported data. The blockade of the S1P signalling in SK1+ cells by $S1P_1$ and $S1P_4$ specific antagonists partially prevented the protective action of S1P (Fig. 9B,C). Notably, the MTT reduction test also revealed a very low and non-significant toxic effect of $A\beta_{42}O$ in SK1+ cells (Fig. 9D). In contrast, blockade of $S1P_1$ and, to a lesser extent, $S1P_4$ evoked a significant reduction in neuronal viability after 24 h (by 23 ± 5% and 20 ± 6%, respectively) as compared to untreated cells transfected with pcDNA (Fig. 9D). Overall, these data indicate that endogenous S1P, generated intracellularly by SK1, exerts a beneficial effect mediated by autocrine/paracrine mechanisms in neuronal cells challenged with toxic $A\beta_{42}O$.

Discussion

In this study, we provide evidence on the ability of S1P to significantly prevent dysfunction in primary rat cortical neurons and human neuroblastoma cells by reducing dramatically the Ca^{2+} dyshomeostasis induced by toxic prefibrillar aggregates of $A\beta_{42}$. Oligomeric assemblies of $A\beta_{42}$ are presently considered to be the key toxic agents responsible for neurodegeneration in AD [3,5,41]. Among the various oligomeric species so far characterized for $A\beta_{42}$, the A11-positive oligomers, also referred to as prefibrillar oligomers or A+, are most interesting because they have been shown to destabilize the lipid bilayer of cells [35,54], cause dysfunction to neuroblastoma and pheochromocytoma cells [4,8,18,35,37] and be present in human AD brains [4,38,39].

These species, called here $A\beta_{42}O$, were also previously reported to aberrantly interact with the neuronal membrane, thus destabilizing its integrity and evoking a massive entry of Ca^{2+} ions from the extracellular space [8,11,18,37]. Our results indicate that S1P can protect neuronal cells challenged by $A\beta_{42}O$ from the abnormal increase in intracellular Ca^{2+} concentration and the following events in the toxicity cascade, such as mitochondrial dysfunction and caspase 3 activation. They also show that the protective effect of S1P was maximum at 100 nM, a physiological level that is responsible for the regulation of many intracellular processes triggered by Ca^{2+} signals [25]. Notably, S1P neuroprotection was mediated by $S1P_1$ and $S1P_4$ and, to a minor extent, also by $S1P_3$ and $S1P_5$, as demonstrated by the functional blockade of S1PR using both S1PR antagonists and by siRNA-mediated S1PR silencing. Moreover, the protective effect of S1P was entirely lost in cells transfected with a combination of all siRNAs raised against the S1PR family and a synergistic effect was evident when the various S1PR agonists were co-incubated. The outlined involvement of multiple S1PRs is in agreement with data reported in literature taking into consideration that S1PRs are co-expressed in the same cell type, including neurons [55,56], are coupled to multiple G proteins [55] and dictate multiple but also at times redundant intracellular downstream activated pathways. Actually, $S1P_1$ exclusively couples to G_i, $S1P_3$ to G_i, G_q and G_{12}, and $S1P_4$ and $S1P_5$ couple to G_i and G_{12}, respectively [44]. Among the plethora of intracellular signalling pathways evoked by S1P, our results indicate that the observed neuroprotective pathway is PTX sensitive, and therefore G_i dependent. These findings are in good agreement with the previously reported ability of the selective $S1P_1$ agonist SEW2871 to reduce Aβ-induced caspase-3 activation, hippocampal neuronal death and cognitive impairment in AD rats [57]. In the same vein, more recently, it has been reported that the S1P analogue fingolimod rescues Aβ-induced Ca^{2+} dyshomeostasis in hippocampal neurons through the activation of $S1P_1$ and $S1P_3$ [34]. Interestingly, the phosphorylated form of fingolimod was previously described as a potent neuroprotective agent against $A\beta_{42}O$, able to stimulate the expression of brain-derived neurotrophic factor (BDNF) in neurons [56]. This evidence was further confirmed in mice injected with $A\beta_{42}O$, in which oral treatment with fingolimod restored the physiological levels of BDNF and, as a consequence, ameliorated memory impairment [58]. Importantly, the neuroprotective effect of $S1P_4$, which decreases the neuronal Ca^{2+} overload induced by $A\beta_{42}O$ has been here highlighted for the first time. In this work, we also emphasize the role of $S1P_5$ in the neuroprotective action of S1P. This is in line with the previously reported evidence on the beneficial effect of the $S1P_5$ agonist A-971432 in a non-clinical animal model for AD [59].

Several reports have shown that Ca^{2+} influx can occur through a generic perturbation of the lipid bilayer and by the alteration of the activity of a variety of channels, such as the ionotropic receptors NMDARs [11,12,16,18,36,60], with a prominent role played by the GluN2B subunit of these channels [19]. Here, we provide mechanistic details of the $S1P_1$- and $S1P_4$- and, to a lesser extent, $S1P_3$- and $S1P_5$-mediated neuroprotective action of S1P on $A\beta_{42}O$-induced Ca^{2+} dysregulation. Our results show that GluN2B subunits of extrasynaptic NMDARs are internalized through a dynamin-dependent endocytic process triggered by S1P signalling cascade, mainly occurring upon the activation of $S1P_1$ and $S1P_4$. A very similar effect has been observed in hippocampal neurons, where fingolimod evoked a very rapid relocation of such subunits at synaptic terminals, where their activation is not neurotoxic, but linked to pro-survival actions through activation of long-term potentiation [34]. Phosphorylated fingolimod was reported to induce a significant membrane accumulation of the GluN2B subunit in rat hippocampal slices upon prolonged $S1P_1$ stimulation, associated with the activation of synaptic versus extrasynaptic NMDARs [61]. Collectively, these findings support a dual role for S1P signalling axis in modulating NMDARs: the first one in driving the rapid endocytic dynamin-dependent internalization of extrasynaptic GluN2B subunit, and the second in stimulating their subsequent exposure at synaptic terminals, where such subunits are directly involved in the stimulation of neuroprotective pathways, leading to an

increase in BDNF expression [62]. These conclusions are also in line with the general proposition that the same NMDAR subunit can activate both neuroprotective and neurotoxic cascades, in dependence on its subcellular localization in the context of synapses.

Fingolimod was also described for its ability to prevent the neurotoxicity of NMDA through the activation of $S1P_1$ [63]. Interestingly, such molecule was reported to improve passive avoidance memory retrieval in relevant AD models as well as mem, one of the few available drugs for the symptomatic treatment of mild and severe AD [33]. Accordingly, in this work, we demonstrated the ability of S1P to rescue the abnormal calcium entry evoked by NMDA through the activation of $S1P_1$, $S1P_3$ and $S1P_4$ to a very similar extent of mem in the presence of $A\beta_{42}O$.

Binding of S1P or agonists, such as phospho-fingolimod, to $S1P_1$ results in phosphorylation of its serine-rich C terminus and subsequent internalization via β-arrestin-mediated clathrin-coated vesicles. After being internalized, the receptor can be consequently recycled back to the membrane, although binding of phospho-fingolimod to $S1P_1$ has been shown to induce its polyubiquitination and degradation [64]. Our results, showing that GluN2B subunits are internalized through an endocytic process triggered by S1P signalling mainly via activation of $S1P_1$ and $S1P_4$ and, to a minor extent, $S1P_3$ and $S1P_5$, reinforce the great protective value of S1P against the abnormal activation of extrasynaptic NMDARs in the cytotoxic cascade responsible for neurodegeneration in AD. These findings point the way for future research characterizing the process at the molecular level.

We also provided evidence on the crucial role played by SK1 in promoting Ca^{2+} homeostasis and neuronal survival mediated by S1P against $A\beta_{42}O$-induced neurotoxicity. Indeed, a significant down-regulation of SK1 and SK2 expression was observed in the presence of $A\beta_{42}O$, limiting S1P production and, consequently, its protective effect. Nevertheless, the mRNA expression levels of SPL as well as SPP1 were diminished, suggesting a reduced degradation of S1P over time, although previously reported data support the evidence that the enzymes involved in S1P biosynthesis, and not those responsible for its catabolism, are mainly responsible for the regulation of S1P cellular levels [65]. We also observed that $A\beta_{42}O$ induced a significant decrease in Spns2 expression, further reducing the pro-survival effects of S1PR in neuronal cells. Our data indicate that in neuronal cells challenged by toxic $A\beta_{42}O$, endogenous S1P generated intracellularly by SK1 exerts a beneficial effect mediated by autocrine/-paracrine mechanisms after its extracellular export via the Spns2, according to previous studies in mouse myoblasts [53,66]. Notably, the deleterious intracellular increase in Ca^{2+} levels and the mitochondrial dysfunction induced by $A\beta_{42}O$ were significantly prevented in SK1 overexpressing cells. Our data are in good agreement with previous evidence on the ability of the 25–35 fragment of Aβ to evoke a massive SK1 inactivation and with the finding that SK1 overexpression significantly prevented Aβ-induced neurotoxicity in neuroblastoma cells [67].

In conclusion, our data provide new important insight into the neuroprotective role of S1P against toxic $A\beta_{42}$ prefibrillar aggregates, both when added exogenously or when its endogenous formation is favoured. The present results indicate that S1P, binding to its receptors $S1P_1$, $S1P_3$, $S1P_4$ and $S1P_5$ stimulates the endocytic internalization of the GluN2B-containing NMDARs, thus contributing to preventing the Ca^{2+} influx induced by deleterious $A\beta_{42}$ oligomers. Taken together, our data point at S1P, S1PR agonists and SK1 activators as potential agents with therapeutic value for AD.

Materials and methods

Preparation of $A\beta_{42}O$

$A\beta_{42}O$ were prepared as previously reported [35]. Briefly, the lyophilized peptide (Bachem, Bubendorf, Switzerland) was dissolved in 100% hexafluoro-2-isopropanol to 1 mM. The solvent was then evaporated under nitrogen and $A\beta_{42}$ was resuspended in 50 mM NaOH at 1 mM, and then diluted in PBS to a final concentration of 25 μM. Then, the sample was centrifuged at 22 000 ***g*** for 30 min, the pellet was discarded, and the supernatant was incubated at 25 °C without agitation for 24 h to obtain $A\beta_{42}O$. $A\beta_{42}$ A- oligomers were prepared with the same procedure, at a final $A\beta_{42}$ concentration of 25 μM, after incubation for 4 days [35]. The preparation of $A\beta_{42}$ fibrils was assessed by dissolving the peptide in 50 mM NaOH at 1 mM, and then diluting it in PBS at a final concentration of 50 μM. The sample was then incubated at 25 °C for 24 h under quiescent conditions [35].

All oligomers and fibrils concentrations are reported as monomer equivalents.

Cell culture

Authenticated human SH-SY5Y neuroblastoma cells were purchased from A.T.C.C. (Manassas, VA, USA) and cultured in Dulbecco's modified Eagle's medium (DMEM), F-12 Ham with 25 mM 4-(2-hydroxyethyl) piperazine-1-ethanesulfonic acid (HEPES) and $NaHCO_3$ (1 : 1) supplemented with 10% FBS, 1 mM glutamine and 1% penicillin and streptomycin solution (Sigma-Aldrich, St. Louis, MO,

USA). Cells were maintained in a 5% CO_2 humidified atmosphere at 37 °C and grown until 80% confluence for a maximum of 20 passages, and routinely tested to ensure that they were free from mycoplasma contamination [68]. For all the experiments, FBS was reduced to 0.5%. Primary rat cortical neurons (Thermo Fisher Scientific, Waltham, MA, USA) were plated and maintained in Neurobasal medium (Thermo Fisher Scientific) supplemented with 0.5 mM GlutaMAX (Gibco, Thermo Fisher Scientific) and 2% (v/v) B-27 serum-free complement (Gibco, Thermo Fisher Scientific) at 37 °C in a 5% CO_2 humidified atmosphere. Every 2 days, the medium was partially replaced with a fresh one and the experiments were performed 14 days after plating, as previously reported [18,37,69], reducing GlutaMAX and B-27 serum-free complement concentrations to 0.25 mM and 1% (v/v) respectively.

RNA interference

SH-SY5Y cells seeded on glass coverslips were transfected with 25 nM Stealth RNAi, referred to as control siRNA (Thermo Fisher Scientific), or with 25 nM siRNA against the GluN2B coding gene GRIN2B (Thermo Fisher Scientific), or with 25 nM siRNA against $S1P_1$ (Merck Millipore, Burlington, MA, USA), $S1P_2$ (Merck Millipore), $S1P_3$ (Merck Millipore), $S1P_4$ (Merck Millipore) and $S1P_5$ (Merck Millipore), or with a combination of all the siRNAs raised against S1PRs, using Lipofectamine 3000 (Life Technologies, Carlsbad, CA, USA), according to the manufacturer's instructions, with 7 μL of lipofectamine and 10 μL of 5 $mg{\cdot}L^{-1}$ transferrin in DMEM for 3 h in a 5% CO_2 humidified atmosphere at 37 °C. Then, the transfection medium was replaced with fresh complete culture medium, in which cells were incubated for 72 h.

Cell transfection with SK1 plasmid

To obtain cells overexpressing wild-type SK1, SH-SY5Y were plated onto 60 mm dishes and transfected using a mix of pcDNA3-human SK1-Flag plasmid (kindly provided by S. Pitson) [70] or empty vector (pcDNA) and Lipofectamine 2000 reagent (1 $mg{\cdot}mL^{-1}$) (Life Technologies) as previously described [71]. After 36 h, cells were utilized for the experiments. Overexpression was checked by western blotting analysis employing anti-Flag (Sigma-Aldrich) and anti-SK1 antibodies (ECM Biosciences, Versailles, KY, USA).

Measurement of cytosolic Ca^{2+} levels

In a set of experiments, SH-SY5Y cells plated on glass coverslips were incubated for 15 min with 1 μM ionomycin, or with 3 μM $A\beta_{42}$ M, $A\beta_{42}$ A-, $A\beta_{42}O$ and fibrils. In another set of experiments, $A\beta_{42}O$ were added to the culture medium of SH-SY5Y cells seeded on glass coverslips for 15 min at increasing concentrations (0.1, 0.3, 1, 3 and 10 μM). In one set of experiments, 3 μM $A\beta_{42}O$ were added to the culture medium of SH-SY5Y cells for 5, 10 and 15 min, in the absence or presence of S1P (Calbiochem, San Diego, CA, USA) at 100 nM. In a separate set of experiments, SH-SY5Y cells were pre-treated with 200 $ng{\cdot}mL^{-1}$ PTX for 4 h and then treated with 3 μM $A\beta_{42}O$ in the absence or presence of 100 nM S1P. In another set of experiments, SH-SY5Y cells were pre-treated for 30 min with the selective S1PR antagonists W146 (Avanti Polar Lipids, Alabaster, AL, USA) at 10 μM ($S1P_1$), JTE013 (Avanti Polar Lipids) at 1 μM ($S1P_2$), CAY10444 (Cayman Chemical, Ann Arbor, MI, USA) at 5 μM ($S1P_3$), CYM50358 (kindly gifted by E. Roberts) [72] at 1 μM ($S1P_4$) and VPC23019 (Avanti Polar Lipids) at 1 μM ($S1P_{1/3}$); cells were then treated with $A\beta_{42}O$ at 3 μM for 15 min, in the absence or presence of 100 nM S1P. SH-SY5Y cells were also treated for 15 min with 3 μM $A\beta_{42}O$ in the presence of the selective S1PR agonists SEW2871 (Calbiochem) at 10 μM ($S1P_1$) and CYM50308 (kindly gifted by E. Roberts) at 1 μM ($S1P_4$), respectively. In a separate set of experiments, SH-SY5Y cells were transfected with control siRNA, or with siRNAs against $S1P_1$, $S1P_2$, $S1P_3$, $S1P_4$ and $S1P_5$ and with a combination of all the siRNAs raised against S1PRs as reported in the previous section, and then treated for 15 min with 3 μM $A\beta_{42}O$ in the absence or presence of 100 nM S1P. In a set of experiments, SH-SY5Y cells were treated with 3 μM $A\beta_{42}O$ for 15 min, in the absence or presence of a 60 min pre-treatment with 10 μM mem (Sigma Aldrich), or after transfection with control siRNA or with siRNA against GluN2B. In a separate set of experiments, primary rat cortical neurons were treated with 3 μM $A\beta_{42}O$ for 15 min, in the absence or presence of 100 nM S1P, or with NMDA (Sigma Aldrich) at 1 mM for 15 min, in the absence or presence of 100 nM S1P, and with or without a pre-incubation of 30 min with the selective S1PR antagonists W146 at 10 μM ($S1P_1$), CAY10444 at 5 μM ($S1P_3$), or CYM50358 at 1 μM ($S1P_4$). In another set of experiments, SH-SY5Y cells were pre-incubated for 30 min with 50 μM dyn (Sigma Aldrich), and then treated with 3 μM $A\beta_{42}O$ and 100 nM S1P for 15 min. In a set of experiments, SH-SY5Y cells pre-transfected with pcDNA or with SK1-Flag plasmid were treated for 15 min with 3 μM $A\beta_{42}O$, in the absence or presence of a 30 min pre-incubation with the selective S1PR antagonists W146 at 10 μM ($S1P_1$), and CYM50358 at 1 μM ($S1P_4$).

Cells were then loaded with 4.5 μM fluo-4 AM (Thermo Fisher Scientific) for 10 min and the cytosolic Ca^{2+} levels were detected after excitation at 488 nm by a TCS SP8 scanning confocal microscopy system (Leica Microsystems, Mannheim, Germany), equipped with an argon laser source. A series of 1-μM-thick optical sections (1024 × 1024 pixels) was taken through the cell depth for each sample using a Leica Plan Apo 63× oil immersion

objective, and all sections were projected as a single composite image by superimposition. The confocal microscope was set at optimal acquisition conditions, e.g. pinhole diameters, detector gain and laser powers. Settings were maintained constant for each analysis. Images were then analysed using the IMAGEJ (NIH, Bethesda, MD, USA) software (Rasband 1997–2018). The fluorescence intensities were typically expressed as the percentage of that measured in untreated cells.

MTT reduction inhibition assay

The mitochondrial status of SH-SY5Y cells seeded in 96-well plates was evaluated by the 3-(4,5-dimethylthiazol-2-yl)-2,5-diphenyltetrazolium bromide (MTT) assay, as reported previously [73]. In a set of experiments, increasing concentrations (0.1, 0.3, 1, 3 and 10 μM) of $A\beta_{42}O$ were added for 24 h to the culture medium of SH-SY5Y cells seeded on 96-well plates. In another set of experiments, SH-SY5Y cells were treated for 24 h with $A\beta_{42}O$ at 3 μM in the absence or presence of increasing concentrations (10, 30, 100, 300 nM and 1 μM) of S1P. In the same set of experiments, SH-SY5Y cells were treated for 24 h with $A\beta_{42}O$ at 3 μM following a 15 min pre-incubation with 100 nM S1P. Increasing concentrations (100, 300 nM and 1 μM) of S1P were also tested as a control. In a separate set of experiments, SH-SY5Y cells were treated for 24 h with $A\beta_{42}O$ at 3 μM in the absence or presence of 100 nM S1P, with or without a 30 min pre-treatment with the selective S1PR antagonists W146 at 10 μM($S1P_1$), CAY10444 at 5 μM ($S1P_3$) and CYM50358 at 1 μM ($S1P_4$), and with a combination of all the S1PRs antagonists at the previously reported concentrations. In another set of experiments, SH-SY5Y were transfected with pcDNA or with the SK1-Flag plasmid, and then treated for 24 h with $A\beta_{42}O$ at 3 μM in the absence or presence of a pre-treatment with the selective S1PR antagonists W146 at 10 μM ($S1P_1$) and CYM50358 at 1 μM ($S1P_4$).

After treatment, the culture medium was removed, and the MTT solution was added to the cells for 4 h. The formazan product was then solubilized with cell lysis buffer (20% sodium dodecyl sulfate and 50% *N*,*N*-dimethylformamide, pH 4.7) for 1 h. The absorbance values of blue formazan were determined at 590 nm with the MICROPLATE MANAGER® Software (Bio-Rad, Hercules, CA, USA). Cell viability was typically expressed as the percentage of MTT reduction in treated cells as compared to the untreated ones, unless otherwise indicated.

Caspase-3 activity assay

SH-SY5Y cells plated on six-well plates were treated for 24 h with $A\beta_{42}O$ at 3 μM in the absence or presence of 100 nM S1P; 100 nM S1P alone was also tested as a control. After treatment, cells were washed twice with PBS and lysed for 20 min at 4 °C in 20 mM Tris–HCl buffer (pH 7.4) containing 250 mM NaCl, 2 mM EDTA, 0.1% Triton X-100, 5 $\mu g \cdot mL^{-1}$ aprotinin, 5 $\mu g \cdot mL^{-1}$ leupeptin, 0.5 mM phenylmethylsulfonylfluoride, 4 mM sodium vanadate and 1 mM DTT. The lysis was completed by sonication, and total protein content was determined in the clarified lysates with the Bradford reagent. Aliquots of total proteins were diluted in 50 mM HEPES-KOH buffer (pH 7.0) containing 10% glycerol, 0.1% 3-[(3-cholamidopropyl)-dimethylammonio]-1-propane sulfonate, 2.0 mM EDTA and 10 mM DTT. Caspase-3 activity was determined, as described in [74,75], by incubating a protein sample for 2 h at 37 °C in the presence of 50 μM Ac-DEVD-AFC (fluorimetric substrate; excitation 405 nm and emission 505 nm). To determine non-specific substrate degradation, the assays were also performed by pre-incubating total protein samples for 15 min at 37 °C with or without the specific caspase inhibitor (200 nM Ac-DEVD-CHO) before substrate addition.

Immunostaining of GluN2B subunit of NMDARs

SH-SY5Y seeded on glass coverslips cells were transfected with control siRNA, or with siRNA against $S1P_1$, $S1P_2$, $S1P_3$, $S1P_4$, $S1P_5$ and with a combination of all the siRNAs raised against S1PRs as reported previously, and then treated for 15 min with S1P at 100 nM, or with $A\beta_{42}O$ at 3 μM in the absence or presence of S1P 100 nM. In the same set of experiments, SH-SY5Y cells were also pre-treated for 30 min with 50 μM dyn. Cells were then fixed with 2% (v/v) paraformaldehyde. After washing twice with PBS, the GluN2B subunit was detected with 1 : 400 diluted anti-NMDAε2 antibody (Santa Cruz Biotechnology, Dallas, TX, USA), and subsequently with 1 : 1000 diluted Alexa Fluor 633-conjugated anti-mouse secondary antibodies (Thermo Fisher Scientific). To detect only GluN2B exposed on the cell surface, the plasma membrane was not permeabilized, thus preventing antibody internalization. Fluorescence emission was detected after excitation at 633 nm by the TCS SP8 scanning confocal microscopy system described above. GluN2B-derived fluorescent puncta were counted using IMAGEJ software after subtracting the background and setting constant thresholds for all the analysed images.

Quantitative real-time reverse transcription PCR

SH-SY5Y cells were plated on six-well plates and then treated for 24 h with $A\beta_{42}O$ at 3 μM. Total RNA from SH-SY5Y cells was then extracted using TRI Reagent® (Sigma-Aldrich). Then, 1–2 μg of RNA was reverse transcribed using the high-capacity cDNA reverse transcription kit (Applied Biosystems, Foster City, CA, USA). TaqMan gene expression assays were used to perform real-time PCR

to quantify the mRNA expression of S1P metabolism enzymes (SK1 and SK2), and S1P-specific transporter Spns2. Each measurement was carried out in triplicate using the CFX96 Touch™ Real-Time PCR Detection System (Bio-Rad) as described previously [75,76], by simultaneous amplification of the target sequence together with the housekeeping gene β-actin. The $2^{-\Delta\Delta Ct}$ method was applied as a comparative method of quantification [77], and data were normalized to β-actin expression.

Western blotting analysis

In a set of experiments, increasing concentrations (0.1, 0.3, 1 and 3 μM) of $A\beta_{42}O$ were added for 24 h to the culture medium of SH-SY5Y cells seeded on six-well plates. In another set of experiments, SH-SY5Y cells were plated on six-well plates and then treated for 24 h with $A\beta_{42}O$ at 3 μM. Cells were then collected and lysed 30 min at 4 °C in a buffer containing 50 mM Tris, pH 7.5, 120 mM NaCl, 1 mM EDTA, 6 mM EGTA, 15 mM $Na4P_2O_7$, 20 mM NaF, 1% Nonidet and protease inhibitor cocktail. Then, lysates centrifuged at 10 000 ***g***, 15 min at 4 °C and 15 μg of protein from total cell lysates were used to perform SDS/PAGE and western blotting analysis in order to evaluate with specific antibodies caspase 3 cleavage (Cell Signalling) or expression of SK1 (ECM Biosciences), SK2 (ECM Biosciences), Spns2 (kindly gifted by T. Nishi). PDVF membranes were incubated overnight with the primary antibodies at 4 °C and then with specific secondary antibodies for 1 h at room temperature. The binding of the antibodies with the specific proteins has been detected by chemiluminescence employing Amersham Imager 600 (GE Heathcare, Buckinghamshire, UK). Densitometric analysis was performed by IMAGEJ software.

Statistical analysis

All data were presented as means ± standard error of mean (SEM). Comparisons between the different groups were performed by Student's *t* test or one-way ANOVA followed by Bonferroni's post-comparison test, or *post hoc* test, by using GRAPHPAD PRISM 7.0 software (San Diego, CA, USA) .

Acknowledgements

The authors thank Prof Eduard Roberts (Department of Chemistry, Scripps Institute, La Jolla, CA, USA) for providing CYM50358 and CYM50308, Dr Tsuyoshi Nishi (Department of Biomolecular Science and Regulation, Osaka University, Japan) for providing antibodies against Spns2 and Prof Stuart Pitson (Division of Human Immunology, Institute of Medical and Veterinary Science, Adelaide, Australia) for providing the pcDNA3-human SphK1-Flag plasmid. The work was supported by the Regione Toscana (FAS-Salute 2018, Project PRAMA to FCh), University of Florence (Fondi Ateneo to RC, CB, FCe, PB, FCh, CD and CC) and the Ministry of Education, Universities and Research of Italy (Progetti Dipartimento di Eccellenza to CD and CC). The data presented in the current study were in part generated using the equipment of the Facility of Molecular Medicine, funded by the Ministry of Education, Universities and Research of Italy – Dipartimenti di Eccellenza 2018–2022. Open Access Funding provided by Universita degli Studi di Firenze within the CRUI-CARE Agreement.

Conflict of interest

The authors declare no conflict of interest.

Author contributions

AB conceptualized the study, developed methodology, investigated and visualized the study, wrote the original draft, and wrote, reviewed and edited the manuscript. RC developed methodology, investigated the study, wrote the original draft, wrote, reviewed and edited the manuscript, and acquired funding. GF investigated and visualized the study. CB investigated and visualized the study, and wrote, reviewed and edited the manuscript. FCe, PB and FCh conceptualized the study, wrote, reviewed and edited the manuscript, and acquired funding. CD conceptualized the study, wrote the original draft, wrote, reviewed and edited the manuscript, administrated the project and acquired funding. CC conceptualized the study, wrote the original draft, wrote, reviewed and edited the manuscript, supervised the study, administrated the project and acquired funding.

Peer review

The peer review history for this article is available at https://publons.com/publon/10.1111/febs.16579.

Data availability statement

The authors confirm that all data needed to evaluate the conclusions of this study are available within the article.

References

1 Selkoe DJ, Hardy J. The amyloid hypothesis of Alzheimer's disease at 25 years. *EMBO Mol Med*. 2016;**8**:595–608.
2 Haass C, Selkoe DJ. Soluble protein oligomers in neurodegeneration: lessons from the Alzheimer's amyloid β-peptide. *Nat Rev Mol Cell Biol*. 2007;**8**:101–12.
3 Chiti F, Dobson CM. Protein misfolding, amyloid formation, and human disease: a summary of progress over the last decade. *Annu Rev Biochem*. 2017;**86**:27–68.
4 Kayed R, Head E, Thompson JL, McIntire TM, Milton SC, Cotman CW, et al. Common structure of soluble amyloid oligomers implies common mechanism of pathogenesis. *Science*. 2003;**300**:486–9.
5 Benilova I, Karran E, De Strooper B. The toxic Aβ oligomer and Alzheimer's disease: an emperor in need of clothes. *Nat Neurosci*. 2012;**15**:349–57.
6 Khachaturian ZS. Calcium, membranes, aging, and Alzheimer's disease. Introduction and over-view. *Ann N Y Acad Sci*. 1989;**568**:1–4.
7 Ye CP, Selkoe DJ, Hartley DM. Protofibrils of amyloid beta-protein inhibit specific K+ currents in neocortical cultures. *Neurobiol Dis*. 2003;**13**:177–90.
8 Demuro A, Mina E, Kayed R, Milton SC, Parker I, Glabe CG. Calcium dysregulation and membrane disruption as a ubiquitous neurotoxic mechanism of soluble amyloid oligomers. *J Biol Chem*. 2005;**280**:17294–300.
9 Supnet C, Bezprozvanny I. The dysregulation of intracellular calcium in Alzheimer disease. *Cell Calcium*. 2010;**47**:183–9.
10 Arbel-Ornath M, Hudry E, Boivin JR, Hashimoto T, Takeda S, Kuchibhotla KV, et al. Soluble oligomeric amyloid-beta induces calcium dyshomeostasis that precedes synapse loss in the living mouse brain. *Mol Neurodegener*. 2017;**12**:27.
11 Cascella R, Cecchi C. Calcium dyshomeostasis in Alzheimer's disease pathogenesis. *Int J Mol Sci*. 2021;**22**:4914.
12 Fani G, Mannini B, Vecchi G, Cascella R, Cecchi C, Dobson CM, et al. Aβ oligomers dysregulate calcium homeostasis by mechanosensitive activation of AMPA and NMDA receptors. *ACS Chem Nerosci*. 2021;**12**:766–81.
13 Kuchibhotla KV, Goldman ST, Lattarulo CR, Wu HY, Hyman BT, Bacskai BJ. Abeta plaques lead to aberrant regulation of calcium homeostasis in vivo resulting in structural and functional disruption of neuronal networks. *Neuron*. 2008;**59**:214–25.
14 Thibault O, Pancani T, Landfield PW, Norris CM. Reduction in neuronal L-type calcium channel activity in a double knock-in mouse model of Alzheimer's disease. *Biochim Biophys Acta*. 2012;**1822**:546–9.
15 Wang Y, Mattson MP. L-type Ca^{2+} currents at CA1 synapses, but not CA3 or dentate granule neuron synapses, are increased in 3xTgAD mice in an age-dependent manner. *Neurobiol Aging*. 2013;**35**:88–95.
16 De Felice FG, Velasco PT, Lambert MP, Viola K, Fernandez SJ, Ferreira ST, et al. Abeta oligomers induce neuronal oxidative stress through an N-methyl-D-aspartate receptor-dependent mechanism that is blocked by the Alzheimer drug memantine. *J Biol Chem*. 2007;**282**:11590–601.
17 Alberdi E, Sánchez-Gómez MV, Cavaliere F, Pérez-Samartín A, Zugaza JL, Trullas R, et al. Amyloid beta oligomers induce Ca^{2+} dysregulation and neuronal death through activation of ionotropic glutamate receptors. *Cell Calcium*. 2010;**47**:264–72.
18 Cascella R, Evangelisti E, Bigi A, Becatti M, Fiorillo C, Stefani M, et al. Soluble oligomers require a ganglioside to trigger neuronal calcium overload. *J Alzheimers Dis*. 2017;**60**:923–38.
19 Rönicke R, Mikhaylova M, Rönicke S, Meinhardt J, Schröder UH, Fändrich M, et al. Early neuronal dysfunction by amyloid β oligomers depends on activation of NR2B-containing NMDA receptors. *Neurobiol Aging*. 2011;**32**:2219–28.
20 Hu NW, Klyubin I, Anwyl R, Rowan MJ. GluN2B subunit-containing NMDA receptor antagonists prevent Abeta-mediated synaptic plasticity disruption in vivo. *Proc Natl Acad Sci USA*. 2009;**106**:20504–9.
21 Rammes G, Mattusch C, Wulff M, Seeser F, Kreuzer M, Zhu K, et al. Involvement of GluN2B subunit containing N-methyl-d-aspartate (NMDA) receptors in mediating the acute and chronic synaptotoxic effects of oligomeric amyloid-beta (Abeta) in murine models of Alzheimer's disease (AD). *Neuropharmacology*. 2017;**123**:100–15.
22 Hung SY, Fu WM. Drug candidates in clinical trials for Alzheimer's disease. *J Biomed Sci*. 2017;**24**:47.
23 Soliven B, Miron V, Chun J. The neurobiology of sphingosine 1-phosphate signalling and sphingosine 1-phosphate receptor modulators. *Neurology*. 2011;**76**:S9–14.
24 Jęśko H, Stępień A, Lukiw WJ, Strosznajder RP. The cross-talk between sphingolipids and insulin-like growth factor signalling: significance for aging and neurodegeneration. *Mol Neurobiol*. 2019;**56**:3501–21.
25 Spiegel S, Milstien S. Sphingosine-1-phosphate: an enigmatic signalling lipid. *Nat Rev Mol Cell Biol*. 2003;**4**:397–407.
26 Aguilar A, Saba JD. Truth and consequences of sphingosine-1-phosphate lyase. *Adv Biol Regul*. 2012;**52**:17–30.
27 Spiegel S, Maczis MA, Maceyka M, Milstien S. New insights into functions of the sphingosine-1-phosphate transporter SPNS2. *J Lipid Res*. 2019;**60**:484–9.

28 Rosen H, Gonzalez-Cabrera PJ, Sanna MG, Brown S. Sphingosine 1-phosphate receptor signalling. *Annu Rev Biochem*. 2009;**78**:743–68.

29 Couttas TA, Kain N, Tran C, Chatterton Z, Kwok JB, Don AS. Age-dependent changes to sphingolipid balance in the human hippocampus are gender-specific and may sensitize to neurodegeneration. *J Alzheimers Dis*. 2018;**63**:503–14.

30 He X, Huang Y, Li B, Gong CX, Schuchman EH. Deregulation of sphingolipid metabolism in Alzheimer's disease. *Neurobiol Aging*. 2010;**31**:398–408.

31 Couttas TA, Kain N, Daniels B, Lim XY, Shepherd C, Kril J, et al. Loss of the neuroprotective factor sphingosine 1-phosphate early in Alzheimer's disease pathogenesis. *Acta Neuropathol Commun*. 2014;**2**:9.

32 Ceccom J, Loukh N, Lauwers-Cances V, Touriol C, Nicaise Y, Gentil C, et al. Reduced sphingosine kinase-1 and enhanced sphingosine 1-phosphate lyase expression demonstrate deregulated sphingosine 1-phosphate signalling in Alzheimer's disease. *Acta Neuropathol Commun*. 2014;**2**:12.

33 Hemmati F, Dargahi L, Nasoohi S, Omidbakhsh R, Mohamed Z, Chik Z, et al. Neurorestorative effect of FTY720 in a rat model of Alzheimer's disease: comparison with memantine. *Behav Brain Res*. 2013;**252**:415–21.

34 Joshi P, Gabrielli M, Ponzoni L, Pelucchi S, Stravalaci M, Beeg M, et al. Fingolimod limits acute Aβ neurotoxicity and promotes synaptic versus extrasynaptic NMDA receptor functionality in hippocampal neurons. *Sci Rep*. 2017;**7**:41734.

35 Ladiwala ARA, Litt J, Kane RS, Aucoin DS, Smith SO, Ranjan S, et al. Conformational differences between two amyloid βoligomers of similar size and dissimilar toxicity. *J Biol Chem*. 2012;**287**:24765–73.

36 Evangelisti E, Cascella R, Becatti M, Marrazza G, Dobson CM, Chiti F, et al. Binding affinity of amyloid oligomers to cellular membranes is a generic indicator of cellular dysfunction in protein misfolding diseases. *Sci Rep*. 2016;**6**:32721.

37 Bigi A, Loffredo G, Cascella R, Cecchi C. Targeting pathological amyloid aggregates with conformation-sensitive antibodies. *Curr Alzheimer Res*. 2020;**17**:722–34.

38 Kokubo H, Kayed R, Glabe CG, Yamaguchi H. Soluble Abeta oligomers ultrastructurally localize to cell processes and might be related to synaptic dysfunction in Alzheimer's disease brain. *Brain Res*. 2005;**1031**:222–8.

39 Kokubo H, Kayed R, Glabe CG, Saido TC, Iwata N, Helms JB, et al. Oligomeric proteins ultrastructurally localize to cell processes, especially to axon terminals with higher density, but not to lipid rafts in Tg2576 mouse brain. *Brain Res*. 2005;**1045**:224–8.

40 Mosmann T. Rapid colorimetric assay for cellular growth and survival: application to proliferation and cytotoxicity assays. *J Immunol Methods*. 1983;**65**:55–63.

41 Cenini G, Cecchi C, Pensalfini A, Bonini SA, Ferrari-Toninelli G, Liguri G, et al. Generation of reactive oxygen species by beta amyloid fibrils and oligomers involves different intra/extracellular pathways. *Amino Acids*. 2010;**38**:1101–6.

42 Itagaki K, Hauser CJ. Sphingosine 1-phosphate, a diffusible calcium influx factor mediating store-operated calcium entry. *J Biol Chem*. 2003;**278**:27540–7.

43 Pulli I, Asghar MY, Kemppainen K, Törnquist K. Sphingolipid-mediated calcium signalling and its pathological effects. *Biochim Biophys Acta Mol Cell Res*. 2018;**1865**:1668–77.

44 Blaho VA, Hla T. An update on the biology of sphingosine 1-phosphate receptors. *J Lipid Res*. 2014;**55**:1596–608.

45 Rapizzi E, Donati C, Cencetti F, Pinton P, Rizzuto R, Bruni P. Sphingosine 1-phosphate receptors modulate intracellular Ca^{2+} homeostasis. *Biochem Biophys Res Commun*. 2007;**353**:268–74.

46 Sanna MG, Wang SK, Gonzalez-Cabrera PJ, Don A, Marsolais D, Matheu MP, et al. Enhancement of capillary leakage and restoration of lymphocyte egress by a chiral S1P1 antagonist in vivo. *Nat Chem Biol*. 2006;**2**:434–41.

47 Guerrero M, Urbano M, Velaparthi S, Zhao J, Schaeffer MT, Brown S, et al. Discovery, design and synthesis of the first reported potent and selective sphingosine-1-phosphate 4 (S1P4) receptor antagonists. *Bioorg Med Chem Lett*. 2011;**21**:3632–6.

48 Salomone S, Waeber C. Selectivity and specificity of sphingosine-1-phosphate receptor ligands: caveats and critical thinking in characterizing receptor-mediated effects. *Front Pharmacol*. 2011;**2**:9.

49 Sanna MG, Liao J, Jo E, Alfonso C, Ahn MY, Peterson MS, et al. Sphingosine 1-phosphate (S1P) receptor subtypes S1P1 and S1P3, respectively, regulate lymphocyte recirculation and heart rate. *J Biol Chem*. 2004;**279**:13839–48.

50 Urbano M, Guerrero M, Velaparthi S, Crisp M, Chase P, Hodder P, et al. Discovery, synthesis and SAR analysis of novel selective small molecule S1P4-R agonists based on a (2Z,5Z)-5-((pyrrol-3-yl)methylene)-3-alkyl-2-(alkylimino)thiazolidin-4-one chemotype. *Bioorg Med Chem Lett*. 2011;**21**:6739–45.

51 Ferreira IL, Bajouco LM, Mota SI, Auberson YP, Oliveira CR, Rego AC. Amyloid beta peptide 1–42 disturbs intracellular calcium homeostasis through activation of GluN2B-containing N-methyl-D-aspartate receptors in cortical cultures. *Cell Calcium*. 2012;**51**:95–106.

52 Li S, Jin M, Koeglsperger T, Shepardson NE, Shankar GM, Selkoe DJ. Soluble Abeta oligomers inhibit long-term potentiation through a mechanism involving excessive activation of extrasynaptic NR2B-containing NMDA receptors. *J Neurosci*. 2011;**31**:6627–38.

53 Gomez-Brouchet A, Pchejetski D, Brizuela L, Garcia V, Altié MF, Maddelein ML, et al. Critical role for sphingosine kinase-1 in regulating survival of neuroblastoma cells exposed to amyloid-beta peptide. *Mol Pharmacol*. 2007;**72**:341–9.
54 Kayed R, Sokolov Y, Edmonds B, McIntire TM, Milton SC, Hall JE, et al. Permeabilization of lipid bilayers is a common conformation-dependent activity of soluble amyloid oligomers in protein misfolding diseases. *J Biol Chem*. 2004;**279**:46363–6.
55 O'Sullivan C, Dev KK. The structure and function of the S1P1 receptor. *Trends Pharmacol Sci*. 2013;**34**:401–12.
56 Doi Y, Takeuchi H, Horiuchi H, Hanyu T, Kawanokuchi J, Jin S, et al. Fingolimod phosphate attenuates oligomeric amyloid β–induced neurotoxicity via increased brain-derived neurotrophic factor expression in neurons. *PLoS ONE*. 2013;**8**:e61988.
57 Asle-Rousta M, Oryan S, Ahmadiani A, Rahnema M. Activation of sphingosine 1-phosphate receptor-1 by SEW2871 improves cognitive function in Alzheimer's disease model rats. *EXCLI J*. 2013;**12**:449–61.
58 Fukumoto K, Mizoguchi H, Takeuchi H, Horiuchi H, Kawanokuchi J, Jin S, et al. Fingolimod increases brain-derived neurotrophic factor levels and ameliorates amyloid β-induced memory impairment. *Behav Brain Res*. 2014;**268**:88–93.
59 Clausznitzer D, Pichardo-Almarza C, Relo AL, van Bergeijk J, van der Kam E, Laplanche L, et al. Quantitative systems pharmacology model for Alzheimer disease indicates targeting sphingolipid dysregulation as potential treatment option. *CPT Pharmacometrics Syst Pharmacol*. 2018;**7**:759–70.
60 Evangelisti E, Wright D, Zampagni M, Cascella R, Fiorillo C, Bagnoli S, et al. Lipid rafts mediate amyloid-induced calcium dyshomeostasis and oxidative stress in Alzheimer's disease. *Curr Alzheimer Res*. 2013;**10**:143–53.
61 Attiori-Essis S, Laurier-Laurin ME, Pépin É, Cyr M, Massicotte G. GluN2B-containing NMDA receptors are upregulated in plasma membranes by the sphingosine-1-phosphate analog FTY720P. *Brain Res*. 2015;**1624**:349–58.
62 Lynch G, Baudry M. Brain and memory: old arguments and new perspectives. *Brain Res*. 2015;**1621**:1–4.
63 Di Menna L, Molinaro G, Di Nuzzo L, Riozzi B, Zappulla C, Pozzilli C, et al. Fingolimod protects cultured cortical neurons against excitotoxic death. *Pharmacol Res*. 2013;**67**:1–9.
64 Nincheri P, Bernacchioni C, Cencetti F, Donati C, Bruni P. Sphingosine kinase-1/S1P1 signalling axis negatively regulates mitogenic response elicited by PDGF in mouse myoblasts. *Cell Signal*. 2010;**22**:1688–99.
65 Cencetti F, Bruno G, Bernacchioni C, Japtok L, Puliti E, Donati C, et al. Sphingosine 1-phosphate lyase blockade elicits myogenic differentiation of murine myoblasts acting via Spns2/S1P2 receptor axis. *Biochim Biophys Acta Mol Cell Biol Lipids*. 2020;**1865**:158759.
66 Bernacchioni C, Cencetti F, Blescia S, Donati C, Bruni P. Sphingosine kinase/sphingosine 1-phosphate axis: a new player for insulin-like growth factor-1-induced myoblast differentiation. *Skelet Muscle*. 2012;**2**:15.
67 Yang Y, Wang M, Lv B, Ma R, Hu J, Dun Y, et al. Sphingosine kinase-1 protects differentiated N2a cells against β-amyloid 25–35-induced neurotoxicity via the mitochondrial pathway. *Neurochem Res*. 2014;**39**:932–40.
68 Limbocker R, Staats R, Chia S, Ruggeri FS, Mannini B, Xu CK, et al. Squalamine and its derivatives modulate the aggregation of amyloid-β and α-synuclein and suppress the toxicity of their oligomers. *Front Neurosci*. 2021;**15**:680026.
69 Bigi A, Ermini E, Chen SW, Cascella R, Cecchi C. Exploring the release of toxic oligomers from α-synuclein fibrils with antibodies and STED microscopy. *Life (Basel)*. 2021;**11**:431.
70 Pitson SM, D'andrea RJ, Vandeleur L, Moretti PA, Xia P, Gamble JR, et al. Human sphingosine kinase: purification, molecular cloning and characterization of the native and recombinant enzymes. *Biochem J*. 2000;**350**:429–41.
71 Bernacchioni C, Ghini V, Cencetti F, Japtok L, Donati C, Bruni P, et al. NMR metabolomics highlights sphingosine kinase-1 as a new molecular switch in the orchestration of aberrant metabolic phenotype in cancer cells. *Mol Oncol*. 2017;**11**:517–33.
72 Cencetti F, Bernacchioni C, Tonelli F, Roberts E, Donati C, Bruni P. TGFβ1 evokes myoblast apoptotic response via a novel signaling pathway involving S1P4 transactivation upstream of Rho-kinase-2 activation. *FASEB J*. 2013;**27**:4532–46.
73 Cascella R, Chen SW, Bigi A, Camino JD, Xu CK, Dobson CM, et al. The release of toxic oligomers from α-synuclein fibrils induces dysfunction in neuronal cells. *Nat Commun*. 2021;**12**:1814.
74 Bruno M, Rizzo IM, Romero-Guevara R, Bernacchioni C, Cencetti F, Donati C, et al. Sphingosine 1-phosphate signaling axis mediates fibroblast growth factor 2-induced proliferation and survival of murine auditory neuroblasts. *Biochim Biophys Acta Mol Cell Res*. 2017;**1864**:814–24.
75 Bruno G, Cencetti F, Bernacchioni C, Donati C, Blankenbach KV, Thomas D, et al. Bradykinin mediates myogenic differentiation in murine myoblasts through the involvement of SK1/Spns2/S1P2 axis. *Cell Signal*. 2018;**45**:110–21.

76 Bernacchioni C, Ghini V, Squecco R, Idrizaj E, Garella R, Puliti E, et al. Role of sphingosine 1-phosphate signalling axis in muscle atrophy induced by TNFα in C_2C1_2 myotubes. *Int J Mol Sci*. 2021;**22**:1280.

77 Livak KJ, Schmittgen TD. Analysis of relative gene expression data using real-time quantitative PCR and the 2(-Delta Delta C(T)) Method. *Methods*. 2001;**25**:402–8.